Nonlinear and stochastic analysis of dynamical instabilities based on Chebyshev polynomial properties and applied to a mechanical system with friction

Alexy Mercier, Louis Jézéquel

▶ **To cite this version:**

Alexy Mercier, Louis Jézéquel. Nonlinear and stochastic analysis of dynamical instabilities based on Chebyshev polynomial properties and applied to a mechanical system with friction. Mechanical Systems and Signal Processing, 2023, 189, pp.110051. 10.1016/j.ymssp.2022.110051 . hal-04496380

HAL Id: hal-04496380
https://hal.science/hal-04496380v1

Submitted on 8 Jan 2025

HAL is a multi-disciplinary open access archive for the deposit and dissemination of scientific research documents, whether they are published or not. The documents may come from teaching and research institutions in France or abroad, or from public or private research centers.

L'archive ouverte pluridisciplinaire **HAL**, est destinée au dépôt et à la diffusion de documents scientifiques de niveau recherche, publiés ou non, émanant des établissements d'enseignement et de recherche français ou étrangers, des laboratoires publics ou privés.

Distributed under a Creative Commons Attribution - NonCommercial 4.0 International License

Version of Record: https://www.sciencedirect.com/science/article/pii/S0888327022011190
Manuscript_1c14ab4f3f6928f94acd5ff0370faec2

Mechanical Systems and Signal Processing 189 (2023) 110051

Contents lists available at ScienceDirect

Mechanical Systems and Signal Processing

journal homepage: www.elsevier.com/locate/ymssp

Nonlinear and stochastic analysis of dynamical instabilities based on Chebyshev polynomial properties and applied to a mechanical system with friction

Alexy Mercier *, Louis Jézéquel

LTDS, École Centrale Lyon, Ecully, France

ARTICLE INFO

Communicated by M. Beer

Keywords:
Friction induced vibrations
Uncertainties
Stochastic problem
Intrusive approach
Chebyshev polynomial
Temporal integration

ABSTRACT

In this paper, mechanical systems presenting instabilities induced by friction such as brakes and clutches are studied using a phenomenological model. For these systems, the stability and vibration levels are strongly linked to the values of certain parameters such as the friction coefficient, contact stiffness, etc. Therefore, it is particularly important to take into account the uncertainties of these parameters to obtain robust and predictive models. In this paper, the modelling of uncertainties is done using probabilistic theory with a parametric view. Each quantity that is a function of the random variables is decomposed in a basis using polynomial chaos. For the model studied, the choice of a classical intrusive approach to solve the mechano-stochastic problem induces particularly long computation times. This is due to the need to perform probabilistic numerical integrations to determine integral terms associated with generalized stochastic forces. As the integration steps in these numerical quadratures must be very small, the calculation times are very long. This is why, in this paper, a modified intrusive approach is presented with the main objective of solving a mechano-stochastic problem in reasonable times and thus avoiding approximation of stochastic generalized forces with numerical integrations. This modified intrusive approach is composed of two parts. In the first part, an approximation of the mechanical action torsor (forces and moments) at the contact and friction interface, is performed. To achieve this, behaviour laws (between torsors) are constructed using potentials and dissipation functions based on physical considerations and reinforced by an influence study. In the second part, the properties of *Chebyshev* polynomials of the second kind are exploited to avoid numerical integration, several times per time step, of the terms associated with generalized stochastic forces. This approach is initially used in a linear framework to perform a stability study of fixed points. It is then used in a nonlinear framework to carry out temporal integrations. Finally, the results of temporal integration and simulation times from the modified intrusive approach are compared to those of the non-intrusive approach. For the latter, *Chebyshev* polynomials of the second kind are also used to interpolate the results of deterministic temporal integrations.

1. Introduction

The objects of study of this article are mechanical systems subjected to vibrations induced by friction [1,2]. The most famous examples are braking systems (automobiles [3], aeronautics [4–6] railways [7]) and clutches [8,9], which have been the subject of

* Corresponding author.
E-mail addresses: alexy.mercier@ec-lyon.fr (A. Mercier), louis.jezequel@ec-lyon.fr (L. Jézéquel).

https://doi.org/10.1016/j.ymssp.2022.110051
Received 9 November 2022; Accepted 14 December 2022
Available online 4 January 2023
0888-3270/© 2023 The Authors. Published by Elsevier Ltd. This is an open access article under the CC BY license (http://creativecommons.org/licenses/by/4.0/).

© 2022 published by Elsevier. This manuscript is made available under the CC BY NC user license
https://creativecommons.org/licenses/by-nc/4.0/

much research. The physical mechanisms causing these vibrations have been studied extensively, in particular stick–slip [10–15] and sprag-slip [16]. The design of these mechanical systems must often satisfy very strict vibration requirements linked to the existence of instabilities and associated vibration levels. For financial reasons, major designers used numerical simulation, which requires knowledge of the main physical phenomena to be introduced in the models. In the case of vibrations induced by friction, the origin of the instabilities is located in the adhesion/friction zones between the rotating and fixed parts. Consequently, the main physical phenomena are unilateral contact and sticking/sliding with friction. Several works based on phenomenological models have shown the importance of taking these phenomena into account [17–22]. Some of the parameters associated with these major phenomena, such as contact stiffness and friction coefficient, present uncertainties and have a strong influence on stability and vibration amplitudes. Consequently, it is essential to take these uncertainties into account in the models. In general, uncertainties can be linked to a lack of information (epistemic uncertainties) or the natural variability (intrinsic uncertainties) of parameters such as those mentioned in [23,24]. The probabilistic theory is that most often used and the most successful for modelling uncertainties and we make use of it in this paper. It makes it possible to represent the probabilistic content of a physical problem by introducing a probabilistic space and then choosing either a parametric [25] or a non-parametric [26,27] view depending on the sources of uncertainty (parameters, geometry, modelling hypotheses, etc.). The polynomial chaos method initiated in 1938 [28] in infinite dimension with extensions [29,30], later applied in finite dimension [31,32], and also generalized [33], is very often used in probabilistic approaches. It will be used in this paper. It consists in decomposing the quantities of interest, which are functions of the random variables, in a basis of multi-dimensional orthogonal polynomials. From the polynomial chaos, a mechano-stochastic problem can be solved using two types of approach: intrusive or non-intrusive. The intrusive approach consists in directly introducing the uncertainties in the equations of the problem. First, a spatial discretization of the material domain is performed and then followed by a spatial approximation of the solution and an initial *Galerkin* projection. Then, the probabilistic approximation of the solution is performed using the polynomial chaos method followed by a second *Galerkin* projection. This second projection makes it possible to project the spatially approximated mechano-stochastic problem on the probabilistic approximation subspace generated by a finite number of multi-dimensional orthogonal polynomials. Finally, a single temporal integration with an adapted finite difference scheme is necessary to obtain quantities of interest such as temporal evolutions associated with displacements, means and even standard deviations. The non-intrusive approach first consists in solving, by temporal integration, a succession of mechano-deterministic problems for a finite number of values of random variables. Then, the results from determinist temporal integrations are either interpolated (projection method [34]) or approximated (regression method [35–39]) using polynomial chaos.

The study carried out in this article is performed on a phenomenological model which includes the main physical mechanisms related to instabilities induced by friction and in particular mode coupling. This model consists of a clamped beam on which a stator disc is mounted. This model also includes a rotor disc rubbing on the stator. The uncertainties of two parameters having a strong influence on stability and vibration levels are taken into account in the model. This is the contact stiffness and the coefficient of friction at the interface of the rotor and stator discs. *Chebyshev* polynomials of the second kind are used to form the basis with polynomial chaos. Indeed, as values of parameters are bounded in engineering, the associated probability density (weight function of the Chebyshev polynomials of the second kind) is very well adapted. Expressions of generalized stochastic forces are complex because of the expressions for the forces and moments at the interface of the discs, the use of polynomial chaos and the *Galerkin* projection. Consequently, it is necessary to perform numerical integrations to calculate these expressions, several per time step, during the temporal integration. Nevertheless, the numerical integration step must be very low due to a slow convergence, which induces very long resolution times. This is why the main objective of this article is to propose a modification of the classic intrusive approach to avoid numerical integrations and thus reduce calculation times. This modified approach consists of two steps. The first consists in simplifying the mathematical expressions of the forces and moments at the interface of the rotor and stator discs. To do this, laws of behaviour linking primal and dual variables are established from physical reasoning reinforced by a study of influence. The simplifications make it possible to carry out the second step, which consists in using certain properties of *Chebyshev* polynomials of the second kind such as [40–44], to directly determine expressions of the stochastic generalized forces without numerical integration.

First, the mechano-stochastic problem is established and all the associated hypotheses are listed. Then, the difficulties related to solving the problem with a classic intrusive approach are detailed after which the modified intrusive approach is presented and fully detailed in two sections. In the first of these sections, the modified intrusive approach is used for a fixed point stability study in a linear framework. Then, in the second of these sections, the modified intrusive approach is presented and used in a nonlinear framework. Finally, the results from the modified intrusive approach are compared with those from a non-intrusive approach in which *Chebyshev* polynomials of the second kind are used to interpolate the results from several temporal integrations of the mechano-deterministic problem, as in [45].

2. Model presentation and main hypothesis

The phenomenological model used for this study is represented in Fig. 1. This is a mechanical system moving in Euclidean space $\mathbb{E}$ during a time interval $T = [0, t_{max}] \subset \mathbb{R}$ and is composed of a clamped beam, denoted b, upon which is mounted a stator disc denoted s in contact with a rotor disc, r. Its movement is measured in the Galilean framework designated by R_0 thanks to the Cartesian coordinate system $\mathcal{R}_0 = (O, \mathcal{B}_0)$ where $\mathcal{B}_0 = (\boldsymbol{e_1}, \boldsymbol{e_2}, \boldsymbol{e_3})$ is the canonical basis of $\mathbb{R}^3$. The associated parameters are given in Table 1 and two among them present uncertainties: the contact stiffness $\varkappa$ and the friction coefficient μ at the interface $(r - s)$,

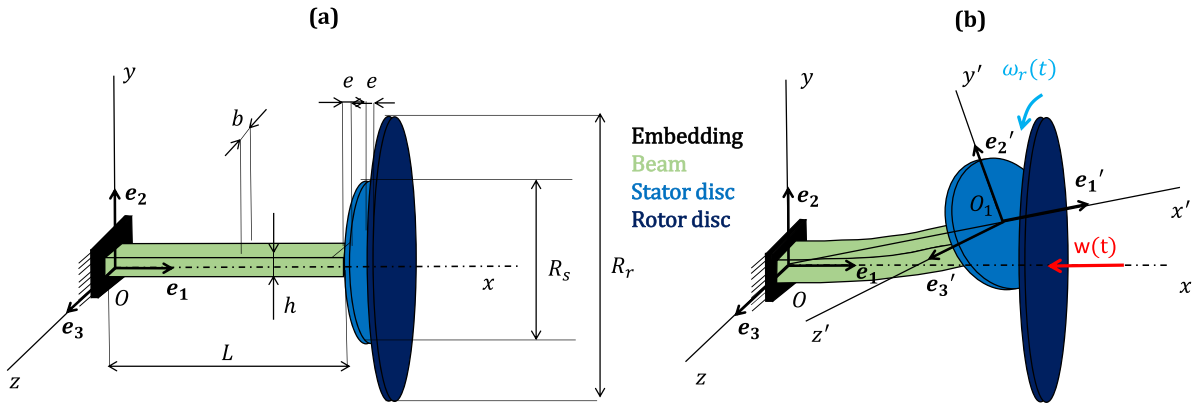

Fig. 1. Diagram of the mechanical system. (a) System in the initial state with geometric parameters whose values are indicated in Table 1. (b) System in motion with a displacement w following x imposed on the rotor disc rotating around x at an angular velocity ω_r.

Table 1
Values of constant parameters appearing in Fig. 1.

Parameter name	Notation	Value	Unit
System density	ρ	7800	kg m^{-3}
Thickness of the beam following y	b	$2.5\,10^{-2}$	m
Thickness of the beam following z	h	$3\,10^{-2}$	m
Beam length	L	$2\,10^{-1}$	m
Contact stiffness per area unit	k	$1\,10^{9}$	N m^{-3}
Young modulus	E	$210\,10^{9}$	Pa
Coulomb modulus	G	$81\,10^{9}$	Pa
Thickness of the rotor and stator discs	e	$1\,10^{-2}$	m
Radius of the stator	R_s	$7.5\,10^{-2}$	m
Radius of the rotor	R_r	$+\infty$	m

which are independent. Consequently, two associated random variables denoted ξ_1 and ξ_2 contained in the vector $\boldsymbol{\xi} \in \Theta =]-1,1[^2$, are introduced, such that:

$$\begin{cases} \varkappa : \xi_1 \in]-1,1[\longmapsto \bar{x} + \xi_1 \varkappa_d \in \mathbb{R} \\ \mu : \xi_2 \in]-1,1[\longmapsto \bar{\mu} + \xi_2 \mu_d \in \mathbb{R} \end{cases} \tag{1}$$

where $\bar{x}$ (respectively $\bar{\mu}$) is the mean value and where $\varkappa_d$ (respectively μ_d) for k (respectively μ). Mathematically, the random vector $\boldsymbol{\xi}$ is the image represented by the map $\boldsymbol{\Xi} : \omega \in \Omega \longmapsto \boldsymbol{\xi} = \boldsymbol{\Xi}(\omega) \in \Theta$, where Ω is an unknown universe and ω an event. The probability measure for $\boldsymbol{\Xi}$ is denoted $\mathbb{P}_{\boldsymbol{\Xi}}$ and associated with the following *Chebyshev* probability density of the second kind:

$$f_{\boldsymbol{\Xi}} : \boldsymbol{\xi} \in \Theta \longmapsto \frac{4}{\pi^2} \prod_{i=1}^{2} \sqrt{1-\xi_i^2} \in [0,1] \tag{2}$$

This probability density is very well adapted for engineering problems given that values of parameters are bounded. Thus, it possible to define the following real *Hilbert* space:

$$S = \bigotimes_{i=1}^{2} L^2_{P_{\Xi_i}}(]-1,1[,\mathbb{R}) = \text{span}\left(H_{\boldsymbol{k}} = \bigotimes_{i=1}^{2} U^{(i)}_{k_i}, \quad \boldsymbol{k} = (k_1,k_2) \in \mathbb{N}^2 \right) \tag{3}$$

where $U^{(i)}_{k_i} :]-1,1[\longrightarrow \mathbb{R}$ is the k_i the *Chebyshev* polynomial associated with the random variable ξ_i and proceeding from the following recurrence relation:

$$\forall k_i \in \mathbb{N}^*, \quad U_{k_i+1}(\xi_i) = 2\,\xi_i\,U_{k_i}(\xi_i) - U_{k_i-1}(\xi_i) \quad \text{with} \quad U_0(\xi_i) = 1 \quad \text{et} \quad U_1(\xi_i) = 2\,\xi_i \tag{4}$$

Consequently, $H_{\boldsymbol{k}} = \prod_{i=1}^{2} U^i_{k_i}$ and S is equipped with the following dot product:

$$\langle H_{\boldsymbol{k}} | H_{\boldsymbol{l}} \rangle_{S',S} = \int_{\Theta} H_{\boldsymbol{k}}(\boldsymbol{\xi})\,H_{\boldsymbol{l}}(\boldsymbol{\xi})\,d\mathbb{P}_{\boldsymbol{\Xi}}(\boldsymbol{\xi}) = \begin{cases} 0 & \text{if} \quad \boldsymbol{k} \neq \boldsymbol{l} \\ \\ 1 & \text{else} \end{cases} \tag{5}$$

where $d\mathbb{P}_{\boldsymbol{\Xi}}(\boldsymbol{\xi}) = f_{\boldsymbol{\Xi}}(\boldsymbol{\xi})\,d\boldsymbol{\xi}$ and S' the topological dual of S.

In order to simplify the mechanical problem, a small displacement hypothesis is made. Moreover, the structure occupying the domain $\Omega \subset \mathbb{E}$ is composed of the following parts:

- b is a *Euler–Bernoulli* beam, of length L and section $S_b = b\,h$ and considered infinitely rigid in tension and torsion.
- the stator s is considered non-deformable, with section $S_s = \pi\,R^2$ and thickness e. In order to manage the contact with friction at the interface between the rotor and stator discs denoted $(r-s)$ of domain Γ_c, a Cartesian coordinate system $\mathcal{R}_1 = \left(O_1, \mathcal{B}_1\right)$ where $\mathcal{B}_1 = \left(\boldsymbol{e_1}', \boldsymbol{e_2}', \boldsymbol{e_3}'\right)$, is defined.
- the rotor disc r is also considered non-deformable, and has a rotation velocity ω_r around direction x and a displacement imposed in direction x, which is defined as follows:

$$w : t \in T \longmapsto \begin{cases} \alpha\, t & \text{for} \quad t \in \left[0, t_f\right] \\ w_f & \text{for} \quad t \in T \setminus \left[0, t_f\right] \end{cases} \in \mathbb{R} \quad \text{where} \quad \alpha \leq 0 \quad \text{and} \quad w_f \leq 0 \tag{6}$$

3. Mechano-stochastic problem and approximation

3.1. Mechano-stochastic problem

In agreement with the previous hypotheses, the mechanical and stochastic problem associated with the phenomenological model is the following:

Find the field $\boldsymbol{u} \in U = \mathbb{R}^2 \otimes R \otimes S \otimes V = \left\{v : (x, \xi, t) \in]0, L[\times T \times \Theta \longmapsto \boldsymbol{v}(x, \xi, t) \in \mathbb{R}^2\right\}$ such that:

$$\begin{cases} E\,\boldsymbol{I_b}\,\dfrac{\partial^4 \boldsymbol{u}}{\partial x^4} + \rho\, S^b\,\boldsymbol{I_d}\,\dfrac{\partial^2 \boldsymbol{u}}{\partial t^2} = \boldsymbol{0} & \text{in} \quad]0, L[\times \Theta \times T & \text{(a)} \\ \boldsymbol{u} = \boldsymbol{0} & \text{in} \quad \{0\} \times \Theta \times T & \text{(b)} \\ \dfrac{\partial \boldsymbol{u}}{\partial x} = \boldsymbol{0} & \text{in} \quad \{0\} \times \Theta \times T & \text{(c)} \\ E\,\boldsymbol{I_b}\,\dfrac{\partial^3 \boldsymbol{u}}{\partial x^3} = -M^s\,\boldsymbol{I_d}\,\dfrac{\partial^2 \boldsymbol{u}}{\partial t^2} - \boldsymbol{F} & \text{in} \quad \{L\} \times \Theta \times T & \text{(d)} \\ E\,\boldsymbol{I_b}\,\dfrac{\partial^2 \boldsymbol{u}}{\partial x^2} = \boldsymbol{J_s}\,\dfrac{\partial^3 \boldsymbol{u}}{\partial x\,\partial t^2} - \boldsymbol{C} & \text{in} \quad \{L\} \times \Theta \times T & \text{(e)} \\ \boldsymbol{u} = \boldsymbol{0} & \text{in} \quad]0, L[\times \Theta \times \{0\} & \text{(f)} \\ \dot{\boldsymbol{u}} = \boldsymbol{0} & \text{in} \quad]0, L[\times \Theta \times \{0\} & \text{(g)} \end{cases} \tag{7}$$

with:

- $V = L^2(T, \mathbb{R})$, is the square-integrable space.
- Eq. (7)(a) is the equilibrium of the beam for each section $x \in]0, L[$, equations (b) and (c) are the *Dirichlet* boundary conditions, equations (d) and (e) are the equilibrium of the stator (mixed boundary conditions), and equations (f) and (g) represent the *Dirichlet* initial conditions.
- $\boldsymbol{I_b} = \dfrac{b\,h^3}{12}\,\boldsymbol{e_2} \otimes \boldsymbol{e_2} + \dfrac{b^3\,h}{12}\,\boldsymbol{e_3} \otimes \boldsymbol{e_3} \in \mathcal{M}_{2,2}(\mathbb{R})$, the inertia tensor and $S_b = b\,h$ is the beam section.
- $\boldsymbol{J_s} = \dfrac{\pi\,R_s^4}{4}\left(\boldsymbol{e_2} \otimes \boldsymbol{e_2} + \boldsymbol{e_3} \otimes \boldsymbol{e_3}\right) \in \mathcal{M}_{2,2}(\mathbb{R})$, inertia tensor of stator disc s and $M_s = \rho\,\pi\,R_s^2\,e \in \mathbb{R}$, is the mass of stator disc s.
- $\boldsymbol{F} : (\xi, t) \in \Theta \times T \longmapsto \boldsymbol{f_F}(\boldsymbol{Y}, w) = \mu \varkappa \displaystyle\int_{\bar{\Gamma}_c(t)} \frac{\Delta u_n}{\|\boldsymbol{\Delta \dot{u}_t}\|}\left(\Delta \dot{u}_{t_1}\,\boldsymbol{e_2} + \Delta \dot{u}_{t_2}\,\boldsymbol{e_3}\right) d\bar{\Gamma}_c(t) \in \mathbb{R}^2$, the force applied on the boundary of domain $\bar{\Gamma}_c$ in direction y (respectively z) .
- $\boldsymbol{C} : (\xi, t) \in \Theta \times T \longmapsto \boldsymbol{f_C}(\boldsymbol{Y}, w) = \varkappa \displaystyle\int_{\bar{\Gamma}_c(t)} \left(\left(x_2'\,\boldsymbol{e_2}' + x_3'\,\boldsymbol{e_3}'\right) \wedge \Delta u_n \left(\boldsymbol{e_1} + \mu \frac{\Delta \dot{u}_{t_1}\,\boldsymbol{e_2} + \Delta \dot{u}_{t_2}\,\boldsymbol{e_3}}{\|\boldsymbol{\Delta \dot{u}_t}\|}\right)\right) d\bar{\Gamma}_c(t) \in \mathbb{R}^2$, the moment applied on the boundary of domain $\bar{\Gamma}_c$ around the direction y (respectively z) .
- $\boldsymbol{Y} = \left[\boldsymbol{u_s}, \boldsymbol{\theta_s}, \dot{\boldsymbol{u}}_{\boldsymbol{s}}, \dot{\boldsymbol{\theta}}_{\boldsymbol{s}}\right]^T \in \mathbb{R}^8$, the vector containing the displacement, the rotation and their time derivatives associated with the centre of the stator disc and for each direction. The rotation is linked to the *Euler–Bernoulli* hypothesis, which gives: $\boldsymbol{\theta_s} = \dfrac{\partial \boldsymbol{u}(L, \cdot, \cdot)}{\partial x} \in \left(\tilde{S} \otimes V\right)^2$.

3.2. Spatial and probabilistic approximations

According to the spatial approximation based on the modal synthesis method and a probabilistic approximation based on the use of polynomial chaos with a *Chebyshev* polynomial of the second kind, the weak solution of the dynamic problem (7) is the following:

$$\begin{aligned} \tilde{\boldsymbol{u}} \in \tilde{U}_w &= \left\{ \boldsymbol{v} : (x, \xi, t) \in]0, L[\times \Theta \times T \longmapsto \sum_{p \in I_p} w_{\boldsymbol{p}}(t)\, H_{\boldsymbol{p_3}}(\xi)\, \phi_{p_2\, p_1}(x)\, \boldsymbol{e}_{p_1} = \boldsymbol{\Phi}(x)\, \boldsymbol{\mathcal{H}}(\xi)\, \boldsymbol{w}(t) \in \mathbb{R}^2 \right\} \\ &= \mathbb{R}^2 \otimes \tilde{R}_w \otimes \tilde{S} \otimes V \end{aligned} \tag{8}$$

with:

- $\mathcal{I}_p = \left\{ \boldsymbol{p} = \left(p_1, p_2, \boldsymbol{p_3}\right) \in \mathbb{N}^4 \quad | \quad p_1 \in \{1;2\}, \quad p_2 \in [\![1, N]\!] \quad \text{and} \quad \boldsymbol{p_3} \in \mathcal{I}_k \right\}$, $N \in \mathbb{N}^*$, the first index set.
- $\mathcal{I}_k = \left\{ \boldsymbol{k} = \left(k_1, k_2\right) \in \mathbb{N}^2 \quad | \quad k_1 \leq n_1 \quad \text{and} \quad k_2 \leq n_2 \right\}$, the second index set.
- $\tilde{R}_w \subset R_w = H^2_{0,D}\left(]0, L[, \mathbb{R}\right)$ (respectively $\tilde{S} \subset S$), the approximation of the *Sobolev* space taking into account the *Dirichlet* boundary condition (7) (b) and (c) (respectively the probabilistic *Hilbert* space).
- $\boldsymbol{\Phi} : \boldsymbol{x} \in]0, L[\longmapsto \begin{bmatrix} \phi_{11}(\boldsymbol{x}) & \cdots & \phi_{i1}(\boldsymbol{x}) & \cdots & \phi_{N1}(\boldsymbol{x}) & 0 & \cdots & 0 & \cdots & 0 \\ 0 & \cdots & 0 & \cdots & 0 & \phi_{12}(\boldsymbol{x}) & \cdots & \phi_{i2}(\boldsymbol{x}) & \cdots & \phi_{N2}(\boldsymbol{x}) \end{bmatrix} \in \mathcal{M}_{2,2N}(\mathbb{R})$, the map associated with the spatial eigenfunction named ϕ_{ji}, $(i, j) \in [\![1, N]\!] \times \{1;2\}$ where $N \in \mathbb{N}^*$, determined with the mixed boundary conditions (7) (c) and (d) for which $\boldsymbol{F}$ and $\boldsymbol{C}$ are null. These spatial eigenfunctions represent the bending modes, taking into account each direction y and z.
- $\boldsymbol{\mathcal{H}} : \boldsymbol{\xi} \in \Theta \longmapsto \begin{bmatrix} \mathrm{Diag}_{\boldsymbol{k}_1}, \ldots, \mathrm{Diag}_{\boldsymbol{k}_{\mathrm{card}(\mathcal{I}_k)}}, \mathrm{Diag}_{\boldsymbol{k}_1}, \ldots, \mathrm{Diag}_{\boldsymbol{k}_{\mathrm{card}(\mathcal{I}_k)}} \\ \mathrm{Diag}_{\boldsymbol{k}_1}, \ldots, \mathrm{Diag}_{\boldsymbol{k}_{\mathrm{card}(\mathcal{I}_k)}}, \mathrm{Diag}_{\boldsymbol{k}_1}, \ldots, \mathrm{Diag}_{\boldsymbol{k}_{\mathrm{card}(\mathcal{I}_k)}} \end{bmatrix} \in \mathcal{M}_{2N,m}(\mathbb{R})$ where $\mathrm{card}\left(\mathcal{I}_k\right) = n_1 n_2$, $m = \mathrm{card}\left(\mathcal{I}_p\right) = 2\,\mathrm{card}\left(\mathcal{I}_k\right) N$ and $\mathrm{Diag}_{\boldsymbol{k}} = \mathrm{diag}\underbrace{\left(H_{\boldsymbol{k}}(\xi), \ldots, H_{\boldsymbol{k}}(\xi)\right)}_{\text{N once}}$, $\boldsymbol{k} \in \mathcal{I}_k$, is the map associated with the probabilistic approximation where the map $H_{\boldsymbol{k}}$ is defined in (3). In this study, *Chebyshev* polynomials of the second kind are used, taking their specific properties compared to other possible polynomials into consideration [43].
- $\boldsymbol{w} : T \longrightarrow \left[\boldsymbol{w}_{\boldsymbol{p}_1}(t) \cdots \boldsymbol{w}_{\boldsymbol{p}_{\mathrm{card}(\mathcal{I}_p)}}(t)\right]^T \in \mathbb{R}^m$, the map giving the stochastic generalized coordinates.

The modal and stochastic coordinates are the solutions of the following discrete problem put in state form:

Find the state map $\boldsymbol{X} : t \in T \longmapsto \left[\boldsymbol{w}(t) \quad \dot{\boldsymbol{w}}(t)\right]^T \in \mathbb{R}^n$, where $n = 2m$, such that:

$$\begin{cases} \dot{\boldsymbol{X}} = \boldsymbol{G}(\boldsymbol{X}, \cdot) & \text{in} \quad T \\ \boldsymbol{X} = \boldsymbol{X_0} & \text{in} \quad \{0\} \end{cases} \tag{9}$$

with:

- $\boldsymbol{G} : (\boldsymbol{X}(t), t) \in \mathbb{R}^n \times T \longmapsto \begin{bmatrix} \boldsymbol{0} & \boldsymbol{I} \\ -\boldsymbol{\Omega}^2 & \boldsymbol{0} \end{bmatrix} \begin{bmatrix} \boldsymbol{w}(t) \\ \dot{\boldsymbol{w}}(t) \end{bmatrix} + \begin{bmatrix} \boldsymbol{0} \\ \boldsymbol{W}(t) \end{bmatrix} \in \mathbb{R}^n$, is the vector field giving the temporal variation of state.
- $\boldsymbol{W}^T : t \in T \longmapsto \begin{array}{l} \left\langle \dfrac{d\boldsymbol{\Phi}^T(L)}{dx}\, \boldsymbol{C}(\cdot, t) \middle| \boldsymbol{\mathcal{H}} \right\rangle_{\mathcal{S}'_1, \mathcal{S}_2} + \left\langle \boldsymbol{\Phi}^T(L)\, \boldsymbol{F}(\cdot, t) \middle| \boldsymbol{\mathcal{H}} \right\rangle_{\mathcal{S}'_1, \mathcal{S}_2} \\ = \displaystyle\int_{\Theta} \left(\boldsymbol{C}^T(\boldsymbol{\xi}, t)\, \frac{d\boldsymbol{\Phi}(L)}{dx} + \boldsymbol{F}^T(\boldsymbol{\xi}, t)\, \boldsymbol{\Phi}(L) \right) \boldsymbol{\mathcal{H}}\, d\mathbb{P}_{\boldsymbol{\Xi}}(\boldsymbol{\xi}) \end{array} \in \mathbb{R}^{1 \times m}$, the map associated with stochastic generalized forces where $\mathcal{S}_1 = S^{2N}$ and $\mathcal{S}_2 = S^{2N \times m}$.
- $\boldsymbol{\Omega}^2 = \left\langle E\, \boldsymbol{I_b}\, \dfrac{d^2\boldsymbol{\Phi}}{dx^2} \middle| \dfrac{d^2\boldsymbol{\Phi}}{dx^2} \right\rangle_{\mathcal{R}'_w, \mathcal{R}_w} = E \displaystyle\int_{]0,L[} \frac{d^2\boldsymbol{\Phi}^T}{dx^2}\, \boldsymbol{I_b}^T\, \frac{d^2\boldsymbol{\Phi}}{dx^2}\, dx \in \mathcal{M}_{2N,2N}(\mathbb{R})$, the squared pulsation matrix where $\mathcal{R}_w = R^{2 \times 2N}$.

The knowledge at each instant $t \in \mathbb{T}$ of the state of the mechanical system $\boldsymbol{X}(t)$ is calculated by means of a temporal integration of the differential equations system (9) using the *Runge–Kutta* 4 scheme. These equations define a non-autonomous stochastic dynamical system denoted $\mathcal{S}^{pheno} = \left(\mathbb{R}^n, T, \boldsymbol{\varphi}_t^{\boldsymbol{pheno}}\right)$.

3.3. Classical intrusive approach and disadvantages

Solving of the mechano-stochastic problem (9) can be done using two approaches: either intrusive (solving of the mechano-stochastic model directly), or non-intrusive (several solvings of the mechano-deterministic model then the interpolation of the results). In both cases, the objective is to determine the unique trajectory $\varphi^{pheno}\left(\boldsymbol{X_0}, \cdot\right)$ given implicitly by the dynamic system $\mathcal{S}^{pheno}$ knowing the state at the initial time $t_0 \in T$. The main advantage of the intrusive approach is that only one time integration is needed to obtain quantities such as displacements $\boldsymbol{u_s}$, rotations $\boldsymbol{\theta_s}$, velocities $\dot{\boldsymbol{u}}_{\boldsymbol{s}}$ and angular rotations $\dot{\boldsymbol{\theta}}_{\boldsymbol{s}}$ at the end of the beam in each or around the y directions and z, for all the values of the random variables $\boldsymbol{\xi} \in \Theta$. During the temporal integration with the *Runge–Kutta* 4 scheme, the expressions present in the duality brackets associated with the stochastic generalized forces $\boldsymbol{W}$ must be calculated several times per time step. These duality brackets correspond to double integrals (on the open set Θ) and contain another double integral associated with forces $\boldsymbol{F}$ or moments $\boldsymbol{C}$ on the contact surface with the adhesion/friction of the stator disc s occupying the open domain $\bar{\Gamma}_c$. Because of the complexity of the expressions in the duality brackets, it is necessary to perform a probabilistic numerical integration. The use of the trapezium method enables approaching the stochastic generalized forces as follows:

$$\hat{\boldsymbol{W}}^T = \frac{1}{2} \sum_{i=1}^{M_1} \sum_{j=1}^{M_2} \left(\hat{\boldsymbol{C}}^T(\boldsymbol{\xi_{ij}}, \cdot)\, \frac{\partial \boldsymbol{\Phi}(L)}{\partial x} + \hat{\boldsymbol{F}}^T(\boldsymbol{\xi_{ij}}, \cdot)\, \boldsymbol{\Phi}(L) \right) \boldsymbol{\mathcal{H}}(\boldsymbol{\xi_{ij}}, \cdot) \sqrt{1 - \xi_{1,i}^2}\, \sqrt{1 - \xi_{2,j}^2}\, \Delta\xi_1\, \Delta\xi_2 \quad \in V^{1 \times m} \tag{10}$$

with:

- $\hat{\boldsymbol{C}}(\boldsymbol{\xi_{ij}}, \cdot) = \left(\bar{x} + \xi_{1,i}\, \varkappa_d\right) \displaystyle\sum_{k=1}^{N_1} \sum_{l=1}^{N_2} \left(\left(x'_{2,k}\, \boldsymbol{e_2}' + x'_{3,l}\, \boldsymbol{e_3}' \right) \wedge \Delta u_n(\boldsymbol{x_{kl}}, \cdot) \left(\boldsymbol{e_1} + \mu \frac{\Delta \dot{u}_{t_1}(\boldsymbol{x_{kl}}, \cdot)\, \boldsymbol{e_2} + \Delta \dot{u}_{t_2}(\boldsymbol{x_{kl}}, \cdot)\, \boldsymbol{e_3}}{\| \boldsymbol{\Delta \dot{u}_t}(\boldsymbol{x_{kl}}, \cdot) \|} \right) \right) \Delta x'_2\, \Delta x'_3 \in V^m$

- $\hat{\boldsymbol{F}}(\boldsymbol{\xi_{ij}},\cdot) = \left(\bar{\mu} + \xi_{2,j}\,\mu_d\right)\,\left(\bar{\varkappa} + \xi_{1,i}\,\varkappa_d\right)\,\sum_{k=1}^{N_1}\sum_{l=1}^{N_2}\frac{\Delta u_n(\boldsymbol{x_{kl}},\cdot)}{\|\boldsymbol{\Delta \dot{u}_t}(\boldsymbol{x_{kl}},\cdot)\|}\,\left(\Delta\dot{u}_{t_1}(\boldsymbol{x_{kl}},\cdot)\,\boldsymbol{e_2} + \Delta\dot{u}_{t_2}(\boldsymbol{x_{kl}},\cdot)\,\boldsymbol{e_3}\right)\,\Delta x'_2\,\Delta x'_3 \in V^m$
- $\left(M_1, M_2\right) \in (\mathbb{N}^*)^2$, the number of probabilistic integration points associated with the first (respectively second) random variable ξ_1 (respectively ξ_2).
- $\boldsymbol{\xi_{ij}} = \left(\xi_{1,i}, \xi_{2,j}\right) \in \Theta$, the coordinates of the probabilistic integration point which follow the following relation: $\xi_{1,i} = \xi_{1,1} + i\,\Delta\xi_1$ and $\xi_{2,j} = \xi_{2,1} + j\,\Delta\xi_2\ \forall (i,j) \in [\![1, M_1]\!] \times [\![1, M_2]\!]$.
- $\left(N_1, N_2\right) \in (\mathbb{N}^*)^2$, the number of spatial integration points associated with the first (respectively second) random variable x'_1 (respectively x'_2).
- $\boldsymbol{x'_{kl}} = \left(x_{2,k}, x_{3,l}\right) \in \Theta$, the coordinates of the spatial integration point according to the following relation: $x'_{2,k} = x'_{2,1} + k\,\Delta x'_2$ and $\xi'_{3,l} = x'_{3,1} + l\,\Delta x'_3\ \forall (k,l) \in [\![1, N_1]\!] \times [\![1, N_2]\!]$.

The convergence step for probabilist numerical integration, is very low which induces very long temporal integration times. Probabilistic numerical integration tests of forces $\boldsymbol{F}$ and moments $\boldsymbol{C}$, showed that a numerical integration step of about $\Delta\xi_1 = \Delta\xi_2 = 10^{-6}$ rad was necessary. During a temporal integration, this time step would induce temporal integration times about 6 h. This inconvenience makes it necessary to avoid integrating the expressions associated with stochastic generalized forces $\boldsymbol{W}$ numerically, by proposing a modification of the classical intrusive approach. The latter is fully detailed in Sections 4 and 5. The modification contains two main steps and makes it possible to calculate duality brackets $\boldsymbol{W}$ without performing probabilistic numerical integration. The first step is necessary to carry out the second and consists in simplifying, in polynomial form, the expressions of the mechanical action torsor, that is to say the forces $\boldsymbol{F}$ and moments $\boldsymbol{C}$ at the disc interface $(r-s)$. This first step also allows getting round the need to carry out spatial numerical integrations (in the domain Γ_c) and thus further reducing the calculation times. The second step exploits certain properties of the *Chebyshev* polynomials of the second kind to directly identify the coefficients of each monomial of the left term of the duality brackets $\boldsymbol{W}$. Comparisons with a non-intrusive approach including several deterministic temporal integrations must be carried out to validate the results from the modified intrusive approach. For the non-intrusive approach, other interesting properties of second kind *Chebyshev* polynomials can be exploited to interpolate the results from deterministic temporal integrations.

4. Modified intrusive approach for the linear stochastic problem

4.1. Study of fixed point stability

The first study carried out focuses on the linear stochastic problem. For this purpose, the maps $\boldsymbol{f_F}$ and $\boldsymbol{f_C}$ giving the forces $\boldsymbol{F}$ and the moments $\boldsymbol{C}$ are developed at the first order around $\boldsymbol{Y_e} = \boldsymbol{0}$, which correspond to a fixed point $\boldsymbol{X_e} = \boldsymbol{0}$ (static equilibrium of the mechanical system) for the dynamical system S^{pheno}. This gives:

$$\begin{cases} \tilde{\boldsymbol{F}}^{\boldsymbol{1}} = \dfrac{\partial \boldsymbol{f_F}(\boldsymbol{Y_e})}{\partial \boldsymbol{u_s}}\,\boldsymbol{u_s} + \dfrac{\partial \boldsymbol{f_F}(\boldsymbol{Y_e})}{\partial \dot{\boldsymbol{u}}_{\boldsymbol{s}}}\,\dot{\boldsymbol{u}}_{\boldsymbol{s}} + \dfrac{\partial \boldsymbol{f_F}(\boldsymbol{Y_e})}{\partial \boldsymbol{\theta_s}}\,\boldsymbol{\theta_s} + \dfrac{\partial \boldsymbol{f_F}(\boldsymbol{Y_e})}{\partial \dot{\boldsymbol{\theta}}_{\boldsymbol{s}}}\,\dot{\boldsymbol{\theta}}_{\boldsymbol{s}} = \varkappa\,\mu\,\left(\boldsymbol{K_F}\,\boldsymbol{\mathcal{H}}\,\boldsymbol{w} + \boldsymbol{C_F}\,\boldsymbol{\mathcal{H}}\,\dot{\boldsymbol{w}}\right) \\ \tilde{\boldsymbol{C}}^{\boldsymbol{1}} = \dfrac{\partial \boldsymbol{f_C}(\boldsymbol{Y_e})}{\partial \boldsymbol{u_s}}\,\boldsymbol{u_s} + \dfrac{\partial \boldsymbol{f_C}(\boldsymbol{Y_e})}{\partial \dot{\boldsymbol{u}}_{\boldsymbol{s}}}\,\dot{\boldsymbol{u}}_{\boldsymbol{s}} + \dfrac{\partial \boldsymbol{f_F}(\boldsymbol{Y_e})}{\partial \boldsymbol{\theta_s}}\,\boldsymbol{\theta_s} + \dfrac{\partial \boldsymbol{f_C}(\boldsymbol{Y_e})}{\partial \dot{\boldsymbol{\theta}}_{\boldsymbol{s}}}\,\dot{\boldsymbol{\theta}}_{\boldsymbol{s}} = \varkappa\,\left(\boldsymbol{K_C}\,\boldsymbol{\mathcal{H}}\,\boldsymbol{w} + \boldsymbol{C_C}\,\boldsymbol{\mathcal{H}}\,\dot{\boldsymbol{w}}\right) \end{cases} \in \left(\tilde{S}\otimes V\right)^2 \tag{11}$$

with:

- $\boldsymbol{K_F} = \dfrac{\partial \boldsymbol{f_F}(\boldsymbol{Y_e})}{\partial \boldsymbol{u}}\,\boldsymbol{\Phi}(L) + \dfrac{\partial \boldsymbol{f_F}(\boldsymbol{Y_e})}{\partial \boldsymbol{\theta}}\,\dfrac{\partial \boldsymbol{\Phi}(L)}{\partial x} \in \mathcal{M}_{2,2N}(\mathbb{R})$ (respectively $\boldsymbol{K_C} = \dfrac{\partial \boldsymbol{f_C}(\boldsymbol{Y_e})}{\partial \boldsymbol{u}}\,\boldsymbol{\Phi}(L) + \dfrac{\partial \boldsymbol{f_C}(\boldsymbol{Y_e})}{\partial \boldsymbol{\theta}}\,\dfrac{\partial \boldsymbol{\Phi}(L)}{\partial x}$), the stiffness matrix associated with $\tilde{\boldsymbol{F}}^{\boldsymbol{1}}$ (respectively $\tilde{\boldsymbol{C}}^{\boldsymbol{1}}$).
- $\boldsymbol{C_F} = \dfrac{\partial \boldsymbol{f_F}(\boldsymbol{Y_e})}{\partial \dot{\boldsymbol{u}}}\,\boldsymbol{\Phi}(L) + \dfrac{\partial \boldsymbol{f_F}(\boldsymbol{Y_e})}{\partial \dot{\boldsymbol{\theta}}}\,\dfrac{\partial \boldsymbol{\Phi}(L)}{\partial x} \in \mathcal{M}_{2,2N}(\mathbb{R})$ (respectively $\boldsymbol{C_C} = \dfrac{\partial \boldsymbol{f_C}(\boldsymbol{Y_e})}{\partial \dot{\boldsymbol{u}}}\,\boldsymbol{\Phi}(L) + \dfrac{\partial \boldsymbol{f_C}(\boldsymbol{Y_e})}{\partial \dot{\boldsymbol{\theta}}}\,\dfrac{\partial \boldsymbol{\Phi}(L)}{\partial x}$), the damping matrix associated with $\tilde{\boldsymbol{F}}^{\boldsymbol{1}}$ (respectively $\tilde{\boldsymbol{C}}^{\boldsymbol{1}}$).

By calculating the dot products associated with $\boldsymbol{W} = \boldsymbol{W_F} + \boldsymbol{W_C}$ and using the properties (4), it is possible to obtain the final expression without calculating the integrals:

$$\begin{cases} \tilde{\boldsymbol{W}}_{\boldsymbol{F}}^{(\boldsymbol{1}),T} = \left\langle \boldsymbol{\Phi}^T(L)\,\left(\boldsymbol{K_F}\,\boldsymbol{Q_F}\,\boldsymbol{\mathcal{H}}\,\boldsymbol{w} + \boldsymbol{C_F}\,\boldsymbol{Q_F}\,\boldsymbol{\mathcal{H}}\,\dot{\boldsymbol{w}}\right)\middle|\boldsymbol{\mathcal{H}}\right\rangle_{S'_1,S_2} = \left(\boldsymbol{K_F}\,\boldsymbol{Q_F}\,\boldsymbol{w} + \boldsymbol{C_F}\,\boldsymbol{Q_F}\,\dot{\boldsymbol{w}}\right)^T\,\boldsymbol{\Phi}(L) \\ \tilde{\boldsymbol{W}}_{\boldsymbol{C}}^{(\boldsymbol{1}),T} = \left\langle \dfrac{d\boldsymbol{\Phi}^T(L)}{dx}\,\left(\boldsymbol{K_C}\,\boldsymbol{Q_C}\,\boldsymbol{\mathcal{H}}\,\boldsymbol{w} + \boldsymbol{C_C}\,\boldsymbol{Q_C}\,\boldsymbol{\mathcal{H}}\,\dot{\boldsymbol{w}}\right)\middle|\boldsymbol{\mathcal{H}}\right\rangle_{S'_1,S_2} = \left(\boldsymbol{K_C}\,\boldsymbol{Q_C}\,\boldsymbol{w} + \boldsymbol{C_C}\,\boldsymbol{Q_C}\,\dot{\boldsymbol{w}}\right)^T\,\dfrac{\partial \boldsymbol{\Phi}(L)}{\partial x} \end{cases} \in V^{1\times m} \tag{12}$$

with:

- $\boldsymbol{Q_F} = \bar{\mu}\,\bar{\varkappa} + \dfrac{1}{2}\,\bar{\mu}\,\varkappa_d\,\boldsymbol{P}_{\xi_1} + \dfrac{1}{2}\,\mu_d\,\bar{\varkappa}\,\boldsymbol{P}_{\xi_2} + \dfrac{1}{4}\,\mu_d\,\varkappa_d\,\boldsymbol{P}_{\xi_1,\xi_2} \in \mathcal{M}_{2N,m}(\mathbb{R})$ and $\boldsymbol{Q_C} = \bar{\varkappa} + \dfrac{1}{2}\,\varkappa_d\,\boldsymbol{P}_{\xi_1} \in \mathcal{M}_{2N,m}(\mathbb{R})$, matrix that allows taking into account the properties (4).
- $\boldsymbol{P}_{\xi_2}, \boldsymbol{P}_{\xi_2}, \boldsymbol{P}_{\xi_1,\xi_2} \in \mathcal{M}_{2N,m}(\mathbb{R})$, matrix such that terms $\xi_i\,U^i_{k_i}(\xi_i)$ are replaced by $\begin{cases} U^i_{k_i+1}(\xi_i) + U^i_{k_i-1}(\xi_i) & \text{if} \quad k_i \in \mathbb{N}^* \\ U^i_1(\xi_i) & \text{if} \quad k_i = 0 \end{cases}$ (see expression (4)).

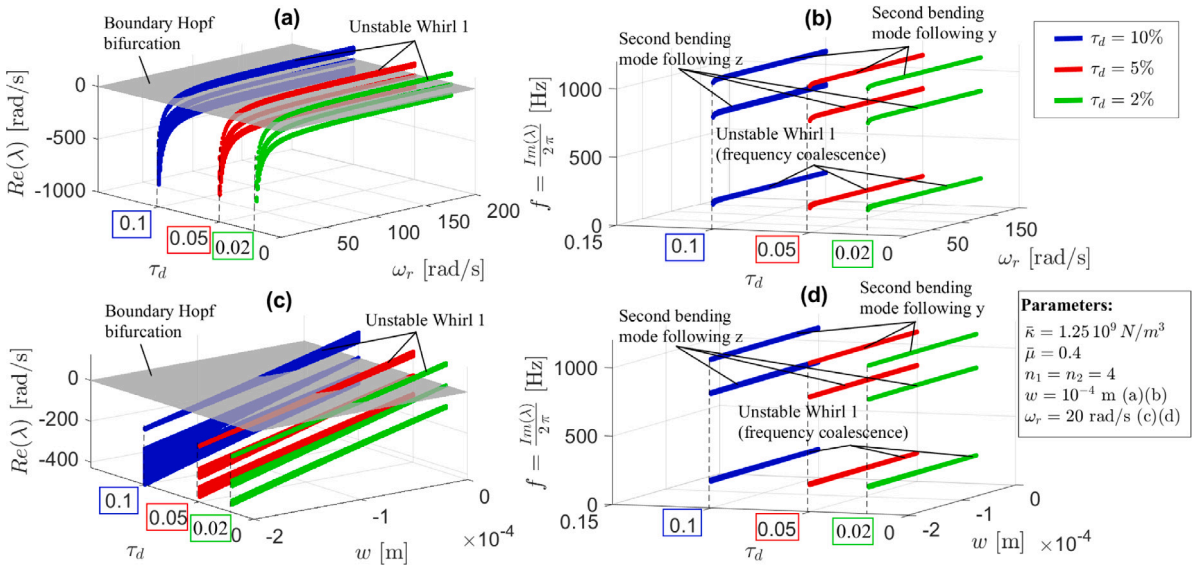

Fig. 2. Stability study of fixed point $\boldsymbol{X_e} = \boldsymbol{0}$ with respect to rotation velocity $\omega_r \in [5, 200]$ rad/s and $w \in [-2\,10^{-4}, 0]$ m and 3 values of dispersal rate $\tau_d \in \{5; 10; 20\}$%. (a)(b) Evolution of real part of eigenvalues Re(λ) and eigenfrequencies $f = \frac{\mathrm{Im}(\lambda)}{2\pi}$ with respect to rotation velocity $\omega_r \in [5, 200]$ rad/s, a fixed displacement $w = -10^{-4}$ m. (c)(d) Evolution of real part of eigenvalues Re(λ) and eigenfrequencies $f = \frac{\mathrm{Im}(\lambda)}{2\pi}$ with respect to displacement $w \in [-2\,10^{-4}, 0]$ m, a fixed velocity rotation $\omega = 20$ rad/s.

Finally, the expression of the stochastic generalized forces is as follows:

$$\tilde{\boldsymbol{W}}^{(1),T} = \left(\boldsymbol{K_F}\,\boldsymbol{Q_F}\,\boldsymbol{w} + \boldsymbol{C_F}\,\boldsymbol{Q_F}\,\dot{\boldsymbol{w}}\right)^T \boldsymbol{\Phi}(L) + \left(\boldsymbol{K_C}\,\boldsymbol{Q_C}\,\boldsymbol{w} + \boldsymbol{C_C}\,\boldsymbol{Q_C}\,\dot{\boldsymbol{w}}\right)^T \frac{\partial \boldsymbol{\Phi}(L)}{\partial x} \quad \in V^{1\times m} \tag{13}$$

First of all, a stability study of the fixed point is carried out by varying parameters w and ω_r. Initially, w is fixed at 10^{-4} m and the stability of $\boldsymbol{X_e} = \boldsymbol{0}$ is studied for a rotation velocity ω_r ranging from 5 to 200 rad/s. Then, a displacement w guaranteeing fixed point stability is chosen and the stability of $\boldsymbol{X_e}$ is studied for a displacement w ranging from 0 to 10^{-4} m. These two studies are carried out for three dispersal rates $\tau_d \in \{2, 5, 10\}$%, giving a dispersion stiffness $\varkappa_d = \tau_d\,\bar{\varkappa}$ and a dispersion friction coefficient $\mu_d = \tau_d\,\bar{\mu}$. Figs. 2(a) and (b) (alongside (c) and (d) respectively) present the evolution of the real parts λ and frequencies f associated with the eigenvalues, according to rotation velocity ω_r (with respect to the displacement of the rotor w), the displacement of the fixed rotor w (with respect to the rotation velocity ω_r) and for three dispersion rates. For the real parts (Fig. 2 (a) and (c)), the equation of plane Re(λ) = 0 is displayed and corresponds to the boundary for which the system S^{pheno} presents a *Hopf* bifurcation (coalescence of frequencies corresponding to a mode coupling with associated levels which amplifies exponentially over time). Moreover, for the ranges of parameters chosen, only the first bending modes of the beam b couple (coalesce around 200 Hz), as shown in Figs. 2 (b) and (d).

4.2. Estimation of the dynamic response in a linear case

The linear response of the mechanical system is studied in the case of transient behaviour. The pair $(w_f, \Omega_r) \in \mathbb{R}^2$ is chosen such that the fixed point is stable. On the other hand, during the displacement ramp represented by $\alpha \in \mathbb{R}$, there is no fixed point, and the points of dynamic equilibrium are not necessarily stable. The objective is to verify its properties and also to study the velocities at which the non-detachment hypothesis is no longer verified, as the linearity hypothesis at the interface $(r - s)$ is valid only if the whole of the surface of the disc is in contact. For this purpose, a temporal integration of the differential equations system is carried out for three velocities $\dot{w} = \alpha$ using the *Rung–Kutta* 4 scheme. For each velocity, the mean, denoted $\bar{u}_{s,1}(t)$, associated with the displacement at the end of beam b and the associated standard deviation $\sigma[u_{s,1}]$ are determined for each instant t_n of the sequence $(t_n)_{n\in I_t}$. Moreover, to verify that the non-detachment hypothesis is satisfied, the mean, $\Delta u_n(\boldsymbol{x_b}, t)$, associated with the normal relative displacement at a point of position vector $\boldsymbol{x}_b$ located at the edge of domain $\Gamma_c(t)$, is determined. In Fig. 3 the temporal evolution of the mean $\bar{u}_{s,1}(t)$3 (a), of the standard deviation $\sigma[u_{s,1}]$3 (b) and relative displacement $\Delta u_n(\boldsymbol{x_b}, t)$3 (c) for three different slope values α are represented. The development of instability is closely related to the slope and is permitted if it is low. In the case of a very high slope, the instability does not have time to develop before critical displacement is reached. In addition, the greater the dispersion rate τ_d, the higher the slope must be to avoid excessive separation and consequently no longer satisfy the associated hypothesis. Finally, it is therefore essential to take nonlinearities into consideration, in particular those related to unilateral contact and friction, when instabilities have time to develop.

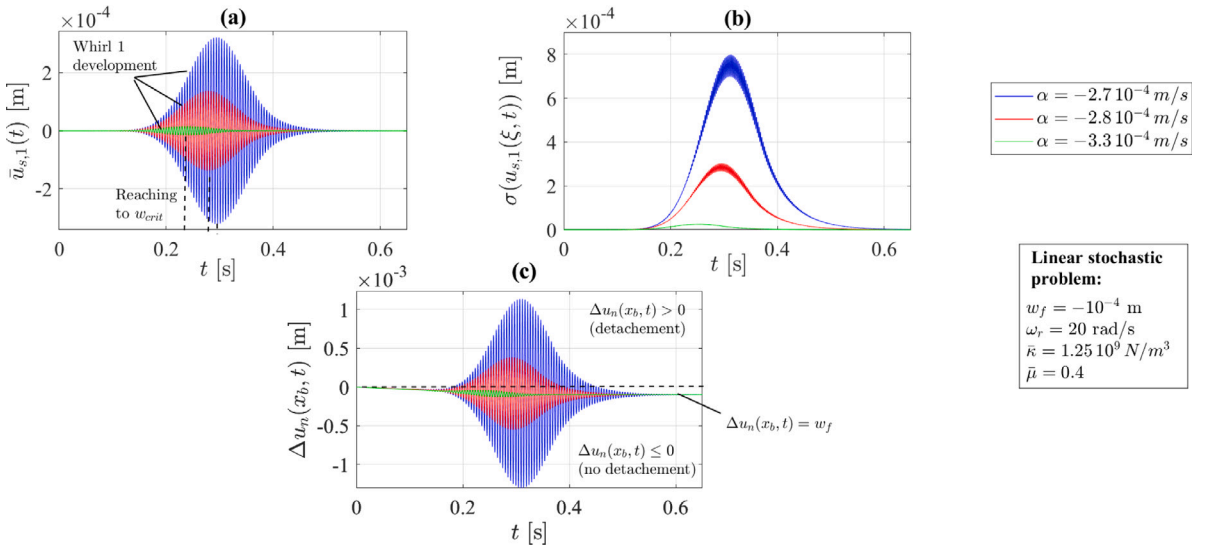

Fig. 3. Stochastic temporal integration around $\boldsymbol{X}_e = \boldsymbol{0}$ for 3 different slopes α. Temporal evolution of the mean $\bar{u}_1$ (a), deviation type $\sigma[u_{s,1}]$ (b) and normal relative displacement $\Delta u_n(\boldsymbol{x_b}, t)$ at the interface $(r-s)$ in $\boldsymbol{x_b} \in \Gamma_c$.

5. Modified intrusive approach for the nonlinear stochastic problem

5.1. Approximations of forces et moments at the interface

As explained previously, if the hypothesis of non-detachment at the interface $(r-s)$ is not satisfied, nonlinear behaviour due to detachment at the interface $(r-s)$ must be taken into account. However, before focusing on stochastic approximation, it is necessary to find simplified expressions of the forces $\boldsymbol{F}$ and moments $\boldsymbol{C}$. Indeed, these forces and moments are expressed in the form of an integral on the interface $(r-s)$ of domain Γ_c, which generates a considerable numerical cost during temporal integration. Moreover, the expression of $\boldsymbol{F}$ and $\boldsymbol{C}$ must be in polynomial form; this will be detailed subsequently. To propose a simplification, it is first necessary to determine the bounds of the intervals to which the variables belong. To do this, four temporal integrations are carried out using the *Runge–Kutta* 4 scheme and are associated with four cases. After integration, the extrema of the variables are determined over the integration interval, which correspond to the limits. The temporal evolution is demonstrated in Fig. 4, and makes it possible to fix the following intervals which corresponds to the extremums: $\theta_{s,1}, \theta_{s,2} \in I_\theta = [-5\,10^{-3}, 5\,10^{-3}]$ rad (Fig. 4 (b) et (f)), $\dot{\theta}_{s,1}, \dot{\theta}_{s,2} \in I_{\dot{\theta}} = [-5, 5]$ rad/s (Fig. 4 (d) et (h)), $u_{s,1}, u_{s,2} \in I_u = [-1\,10^{-3}, 1\,10^{-3}]$ m (Fig. 4 (a) et (e)) and $\dot{u}_{s,1}, \dot{u}_{s,2} \in I_{\dot{u}} = [-1, 1]$ (Fig. 4 (c) et (g)). In the second step, it is necessary to identify the variables which have little or no influence on the forces $\boldsymbol{F}$ and the moment $\boldsymbol{C}$. To achieve this, and as shown in Fig. 5, the forces and moments are plotted as a function of the variables. For the forces, it is easy to see that there is a strong influence exerted by the angles and velocities (Figs. 5 (b) and (c)), a weak influence by the displacements (Fig. 5 (a)) and almost no influence from the angular velocities (Fig. 5 (d)). Concerning the moments, only the angles have a notable influence (Fig. 5 (f)), while the influence of the other variables is limited (Figs. 5 (e), (g) and (h)). In order to reinforce these analyses of the influence of the variables and thus make them more relevant, the partial derivatives of the expressions of the forces and moments with respect to each of the variables are studied. To perform the relevant comparisons, each partial derivative is multiplied by the maximum of the associated variable. This makes it possible to obtain quantities of the same dimension (same unit). Finally, these modified partial derivatives have the following form:

$$\frac{\partial \boldsymbol{F}}{\partial \overline{\boldsymbol{Y}}} = \frac{\partial \boldsymbol{F}}{\partial \boldsymbol{Y}} \boldsymbol{Y}^{max} \quad \text{and} \quad \frac{\partial \boldsymbol{C}}{\partial \overline{\boldsymbol{Y}}} = \frac{\partial \boldsymbol{C}}{\partial \boldsymbol{Y}} \boldsymbol{Y}^{max} \quad \in \left(\tilde{S} \otimes V\right)^{2\times 8} \tag{14}$$

with :

- $\overline{\boldsymbol{Y}} = (\boldsymbol{Y}^{max})^{-1}\ \boldsymbol{Y} \in \mathbb{R}^8 \Longrightarrow \dfrac{\partial \boldsymbol{Y}}{\partial \overline{\boldsymbol{Y}}} = \boldsymbol{Y}^{max} \in \mathbb{R}^{8\times 8}$

Fig. 6 (respectively 7) shows the evolutions of the modified partial derivatives which are associated with the first (and second) bending of beam b. The analysis of these two Figs. 6 and 7 confirms the previous conclusions, i.e. a strong influence of the variables $\boldsymbol{\theta_s}$ and $\boldsymbol{\dot{u}_s}$ (respectively $\boldsymbol{\theta_s}$) for the forces $\boldsymbol{F}$ (respectively moments $\boldsymbol{C}$). These conclusions lead to the following simplifications:

- Approximated moments $\tilde{\boldsymbol{C}} = \boldsymbol{f}_{\tilde{C}}\left(\boldsymbol{\theta_s}, w\right)$ in $\Theta \times T$: these moments are considered dependent only on the angles $\theta_{s,1}$ and $\theta_{s,2}$ as shown in Fig. 5. Given that these components are conservative forces (per unit area), it is advisable to choose a form of

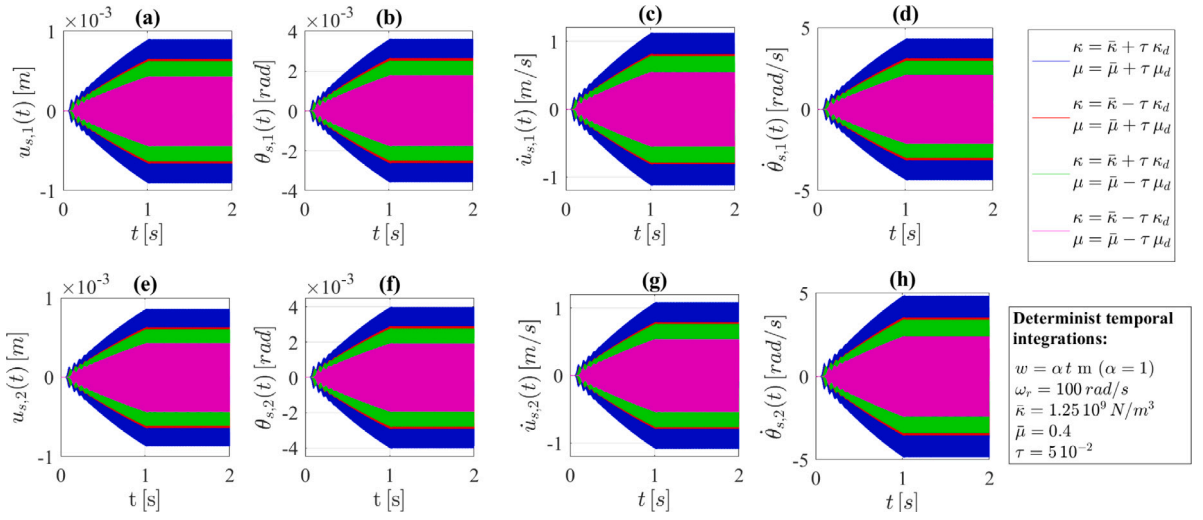

Fig. 4. Temporal integration of problem (9) with *Runge–Kutta* 4 and for 4 pairs (k, μ) with $\tau = 5\,10^{-2}$%. Temporal evolution of $u_{s,1}$ (a), $\theta_{s,1}$ (b), $\dot{u}_{s,1}$ (c), $\dot{\theta}_{s,1}$ (d), $u_{s,2}$ (e), $\theta_{s,2}$ (f), $\dot{u}_{s,2}$ (g), $\dot{\theta}_{s,2}$ (h).

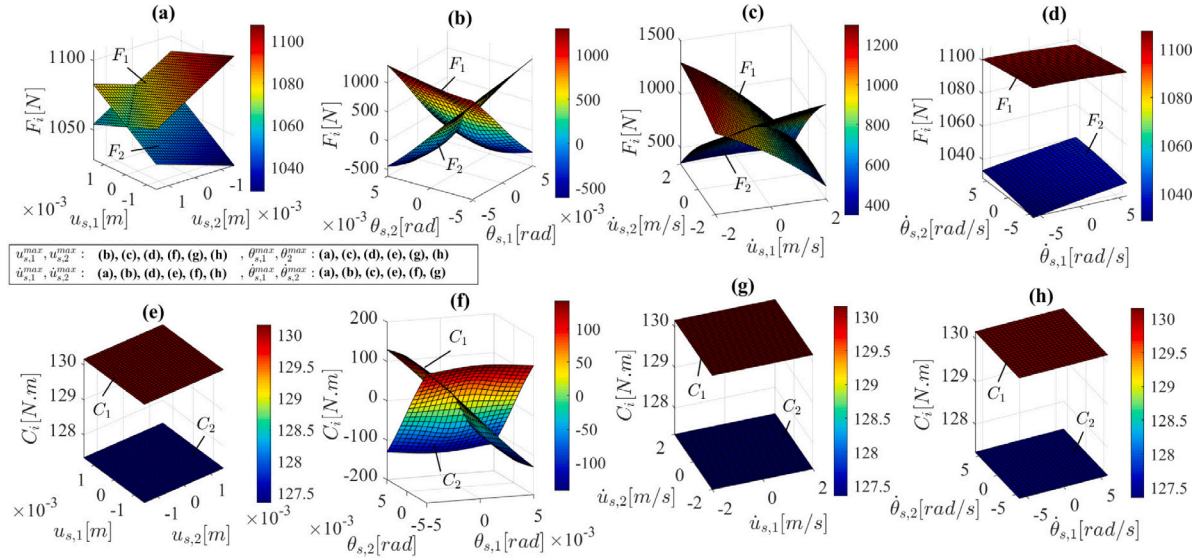

Fig. 5. Influence of displacements $\boldsymbol{u_s}$, rotation $\boldsymbol{\theta_s}$, and their temporal derivative $\boldsymbol{\dot{u}_s}$, $\boldsymbol{\dot{\theta}_s}$ on the forces $\boldsymbol{F}$ and moments $\boldsymbol{C}$. Evolution with respect to $u_{s,1}$ and $u_{s,2}$ for the forces (a) and moments (e), with respect to $\dot{u}_{s,1}$ and $\dot{u}_{s,2}$ for the forces (b) and moments (f), with respect to $\theta_{s,1}$ and $\theta_{s,2}$ for the forces (c) and moments (g) and with respect to $\dot{\theta}_{s,1}$ and $\dot{\theta}_{s,2}$ for the forces (d) and moments (h).

potential energy which is positive-definite:

$$\mathcal{W} = \frac{1}{2}\,\varkappa \sum_{j \in \mathcal{I}_c} A_j(w) \left(\theta_{s,1}^2 + \theta_{s,2}^2\right)^j \quad \in \tilde{S} \otimes V \tag{15}$$

where: $A_j : [w^{min}, w^{max}] \longrightarrow \mathbb{R}$, $j \in \mathcal{I}_c = \{2; 4; \cdots; n_c\} \subset 2\,\mathbb{N}^*$ contains the terms of the series after truncation at index n_c, maps to be determined which are defined on the set of displacements w of the rotor disc in the direction x. Consequently, the simplified polynomial form is the following:

$$\tilde{\boldsymbol{C}} = \sum_{i=2}^{3} \frac{\partial \mathcal{W}}{\partial \theta_{s,i-1}}\, \boldsymbol{e_i} = \varkappa \sum_{i=2}^{3} \left(\sum_{j \in \mathcal{I}_c} (j-1)\, A_j(w) \left(\theta_{s,1}^2 + \theta_{s,2}^2\right)^j \theta_{s,i-1} \right) \boldsymbol{e_i} \quad \in \left(\tilde{S} \otimes V\right)^2 \tag{16}$$

- Forces $\tilde{\boldsymbol{F}} = \boldsymbol{f}_{\tilde{F}}\left(\boldsymbol{\theta_s}, \boldsymbol{\dot{u}_s}, w\right)$ in $\Theta \times T$: These forces are considered dependent only on angles $\theta_{s,1}$ and $\theta_{s,2}$ and the velocity $\dot{u}_1$ (with respect to $\dot{u}_2$) for F_1 (with respect to F_2) as shown in Fig. 5. The form of the forces is associated with physical considerations

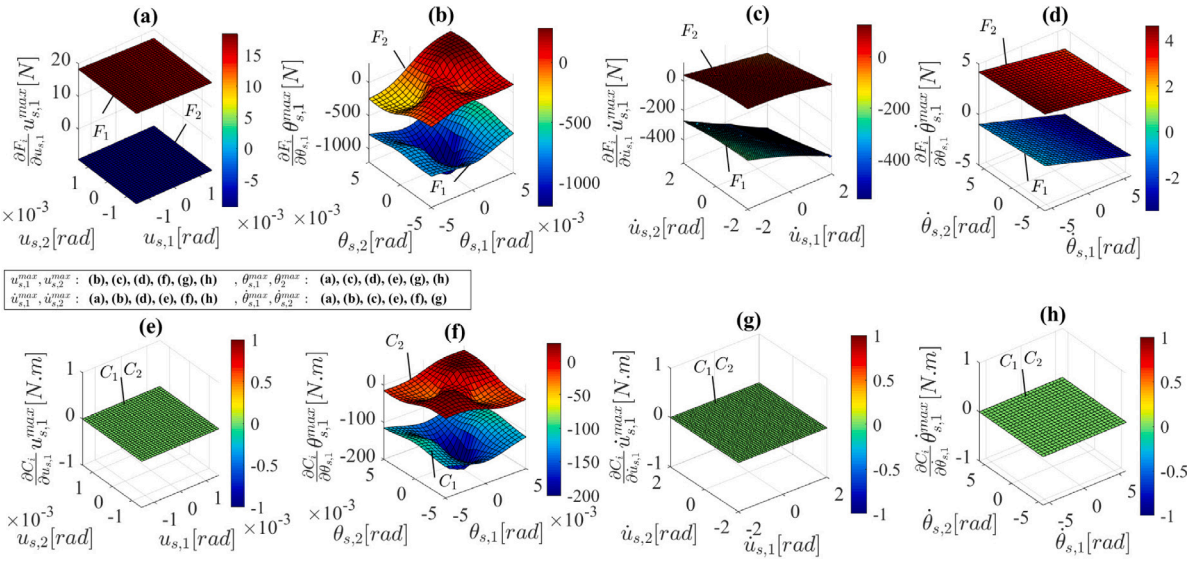

Fig. 6. Influence of displacements $\boldsymbol{u_s}$, rotation $\boldsymbol{\theta_s}$, and their temporal derivative $\dot{\boldsymbol{u}}_{\boldsymbol{s}}$, $\dot{\boldsymbol{\theta}}_{\boldsymbol{s}}$ on the modified partial derivatives $\frac{\partial \boldsymbol{F}}{\partial \overline{\boldsymbol{Y}}_1}$ and moments $\frac{\partial \boldsymbol{C}}{\partial \overline{\boldsymbol{Y}}_1}$. Evolution with respect to $u_{s,1}$ and $u_{s,2}$ for the forces (a) and moments (e), with respect to $\dot{u}_{s,1}$ and $\dot{u}_{s,2}$ for the forces (b) and moments (f), with respect to $\theta_{s,1}$ and $\theta_{s,2}$ for the forces (c) and moments (g) and with respect to $\dot{\theta}_{s,1}$ and $\dot{\theta}_{s,2}$ for the forces (d) and moments (h).

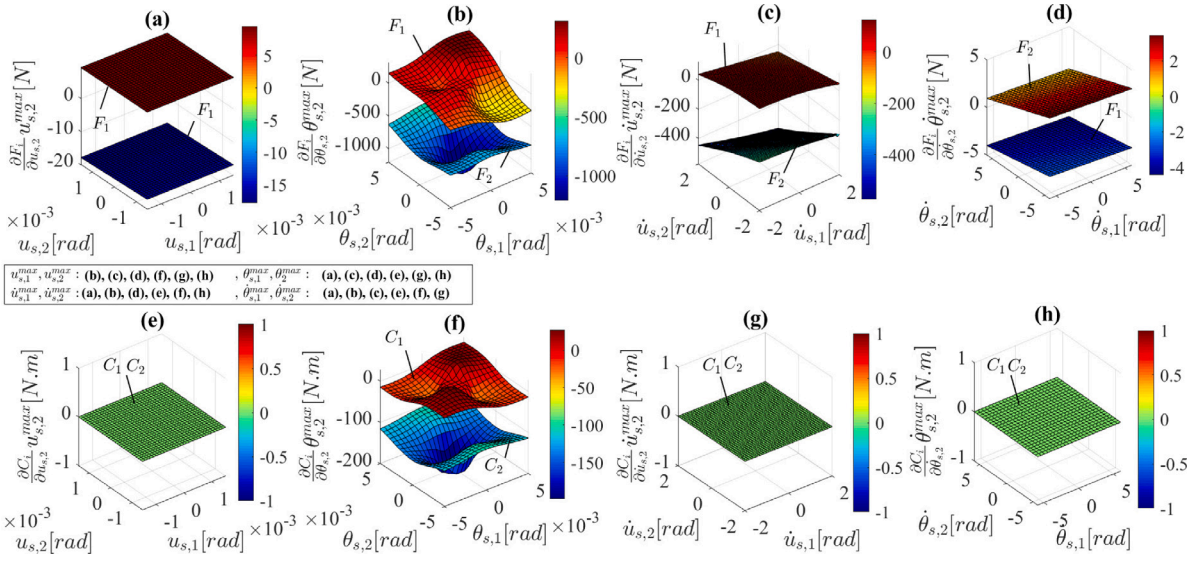

Fig. 7. Influence of displacements $\boldsymbol{u_s}$, rotation $\boldsymbol{\theta_s}$, and their temporal derivative $\dot{\boldsymbol{u}}_{\boldsymbol{s}}$, $\dot{\boldsymbol{\theta}}_{\boldsymbol{s}}$ on the modified partial derivatives $\frac{\partial \boldsymbol{F}}{\partial \overline{\boldsymbol{Y}}_2}$ and moments $\frac{\partial \boldsymbol{C}}{\partial \overline{\boldsymbol{Y}}_2}$. Evolution with respect to $u_{s,1}$ and $u_{s,2}$ for the forces (a) and moments (e), with respect to $\dot{u}_{s,1}$ and $\dot{u}_{s,2}$ for the forces (b) and moments (f), with respect to $\theta_{s,1}$ and $\theta_{s,2}$ for the forces (c) and moments (g) and with respect to $\dot{\theta}_{s,1}$ and $\dot{\theta}_{s,2}$ for the forces (d) and moments (h).

and is composed of two parts. The first is associated with the instability induced by friction and must mainly contain angle $\theta_{s,i}$. The second is associated with the dissipation given by plane friction at the interface $(r-s)$ and must mainly contain angle $\theta_{s,1}$ (with respect to $\theta_{s,2}$) for F_1 (with respect to F_2). Consequently, the expression is the following:

$$\tilde{\boldsymbol{F}} = \mu \varkappa \sum_{i=2}^{3} \left(\sum_{j \in \mathcal{I}_f} \left(B_j(w)\, \theta_{s,i-1} + D_j(w)\, \dot{u}_{s,i-1} \right) \left(\theta_{s,1}^2 + \theta_{s,2}^2 \right)^j \right) \boldsymbol{e_i} \quad \in \left(\tilde{S} \otimes V \right)^2 \tag{17}$$

where: $B_j : [w^{min}, w^{max}] \longrightarrow \mathbb{R}$ and $D_j : [w^{min}, w^{max}] \longrightarrow \mathbb{R}$, $j \in \mathcal{I}_f = \{2; 4; \cdots; n_f\} \subset 2\,\mathbb{N}^*$ contains the terms of the series after truncation at index n_f, maps to be determined defined on the set of displacements w of the rotor disc in direction x.

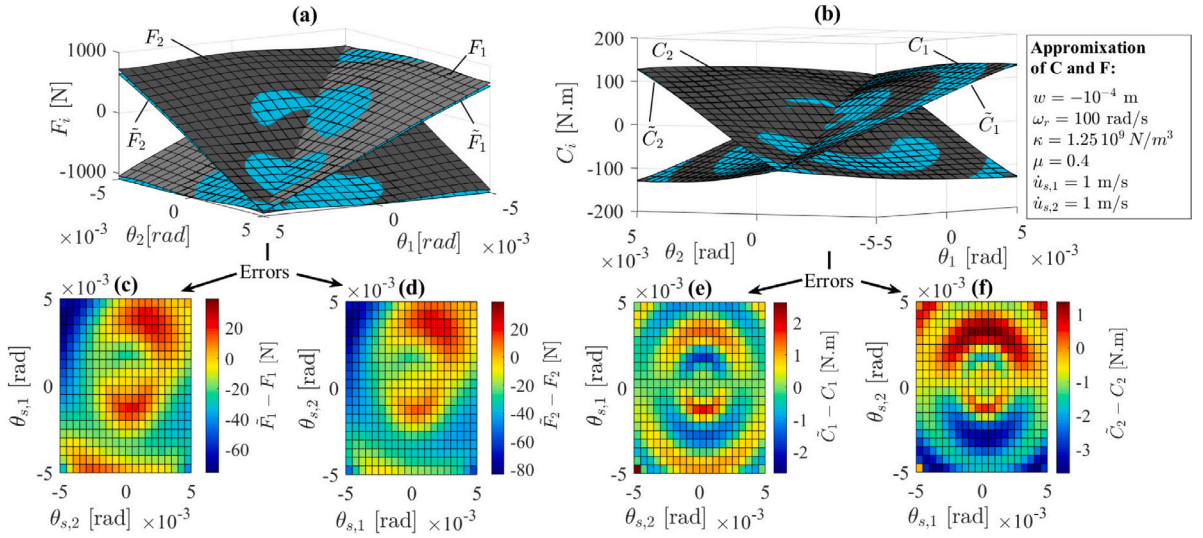

Fig. 8. Comparison to reference $\boldsymbol{F}$ and $\boldsymbol{C}$ and the approximated $\tilde{\boldsymbol{F}}$ and $\tilde{\boldsymbol{C}}$ forces and moments. (a) Comparison of reference (grey) and approximated (blue) forces with errors between F_1 and $\tilde{F}_1$ (c) as well as F_2 and $\tilde{F}_2$ (d). (b) Comparison of reference (grey) and approximated (blue) moments with errors between C_1 and $\tilde{C}_1$ (e) and C_2 and $\tilde{C}_2$ (f).

Then, in the first step, the least squares method is used to approximate and establish the coefficient vectors $\boldsymbol{A}(w)$, $\boldsymbol{B}(w)$ and $\boldsymbol{D}(w)$ for each $w \in [\![w_1, w_n]\!]$, where $w_k = w^{min} + k\,h$ is the term of the arithmetic sequence $(w_k)_{k\in\mathcal{I}_w}$. In the second step, the least squares method is still used to approximate each map $\boldsymbol{A}$, $\boldsymbol{B}$ and $\boldsymbol{D}$. These two steps give rise to the following optimization problem without constraints:

$$\begin{cases} \forall k \in \mathcal{I}_w, \quad \boldsymbol{f}_{lq1}\left(\boldsymbol{A}(w_k), \boldsymbol{B}(w_k), \boldsymbol{D}(w_k)\right) = \min\limits_{\boldsymbol{a}\in\mathbb{R}^{n_c}, \boldsymbol{b},\boldsymbol{d}\in\mathbb{R}^{n_f}} \boldsymbol{f}_{lq1}(\boldsymbol{a},\boldsymbol{b},\boldsymbol{d}) & \text{(Step 1)} \\ \boldsymbol{f}_{lq2}\left(\boldsymbol{c}_a, \boldsymbol{c}_b, \boldsymbol{c}_d\right) = \min\limits_{\boldsymbol{x}_a,\boldsymbol{x}_b,\boldsymbol{x}_d\in\mathbb{R}^3} \boldsymbol{f}_{lq2}\left(\boldsymbol{x}_a, \boldsymbol{x}_b, \boldsymbol{x}_d\right) & \text{(Step 2)} \end{cases} \tag{18}$$

with:

- $\boldsymbol{f}_{lq1} : (\boldsymbol{a},\boldsymbol{b},\boldsymbol{d}) \in \mathbb{R}^{n_c}\times\mathbb{R}^{n_f}\times\mathbb{R}^{n_f} \longmapsto \boldsymbol{f}_{lq1}(\boldsymbol{a},\boldsymbol{b},\boldsymbol{d}) = \left\| \left[\boldsymbol{F}(\boldsymbol{Y}_i, w_k) \quad \boldsymbol{C}(\boldsymbol{Y}_i, w_k)\right]^T - \left[\tilde{\boldsymbol{F}}(\boldsymbol{Y}_i, w_k) \quad \tilde{\boldsymbol{C}}(\boldsymbol{Y}_i, w_k)\right]^T \right\|_2^2 \in \mathbb{R}$, the square of the discrete Euclidean norm of the difference between reference maps $\boldsymbol{F}$ and $\boldsymbol{C}$, and approximated map $\tilde{\boldsymbol{F}}$ and $\tilde{\boldsymbol{C}}$ evaluated in n_{lq1} vector $\boldsymbol{Y}$ where $\theta_{s,1} \in [\theta_{s,1}^{min}, \theta_{s,1}^{max}]$, $\theta_{s,1} = 0$, $\dot{u}_{s,1} \in [\dot{u}_{s,1}^{min}, \dot{u}_{s,1}^{max}]$ and $\dot{u}_{s,2} = 0$.
- $\boldsymbol{f}_{lq2} : \left(\boldsymbol{x}_a, \boldsymbol{x}_b, \boldsymbol{x}_d\right) \in \mathbb{R}^3\times\mathbb{R}^3\times\mathbb{R}^3 \longmapsto \boldsymbol{f}_{lq2}(\boldsymbol{x}_a,\boldsymbol{x}_b,\boldsymbol{x}_d) = \left\| \left[\boldsymbol{A}(w_k)\,\boldsymbol{B}(w_k)\,\boldsymbol{D}(w_k)\right]^T - \sum\limits_{i=0}^{2} \left[\boldsymbol{x}_a\,\boldsymbol{x}_b\,\boldsymbol{x}_d\right]^T w_k^i \right\|_2^2 \in \mathbb{R}$, the square of the discrete Euclidean norm of the difference between the maps and the approximated map (polynomial of degree two) evaluated in each term of the sequence $(w_k)_{k\in\mathcal{I}_w}$.

The previous steps can now be used to find approximations of forces and moments. In Fig. 8 , the reference ($\boldsymbol{F}$ and $\boldsymbol{C}$ in Fig. 8 (a)) and approximated ($\tilde{\boldsymbol{F}}$ and $\tilde{\boldsymbol{C}}$ in Fig. 8 (b)) forces and moments as well as the approximation errors (Fig. 8 (c), (d), (e) and (f)) are plotted, with respect to the angles ($\theta_{s,1}$ and $\theta_{s,2}$) and velocities ($\dot{u}_{s,1}$ and $\dot{u}_{s,2}$). The errors overall demonstrate minor irregularities, which makes it possible to validate the approximations.

5.2. Use of Chebyshev polynomial properties

Once an efficient approximation of the forces and moments in a polynomial form has been obtained, it is possible to apply certain properties of the *Chebyshev* polynomials of the second kind, in order to transform the products (associated with the nonlinearities) into sums. This transformation makes it possible to obtain expressions of forces $\tilde{\boldsymbol{F}}$ and moments $\tilde{\boldsymbol{C}}$ directly in the scope of spatial and probabilistic approximation bases and consequently to avoid a numerical calculation of the integral (corresponding to the inner product) at each time step, which would greatly lengthen the times. Firstly, replacing the expressions of $\boldsymbol{u_s}$, $\boldsymbol{\theta_s}$, $\dot{\boldsymbol{u}}_{\boldsymbol{s}}$ and $\dot{\boldsymbol{\theta}}_{\boldsymbol{s}}$ in (16) and (17), gives us:

$$\begin{cases} \tilde{\boldsymbol{F}} = \mu \varkappa \sum\limits_{\boldsymbol{j}\in\mathcal{I}_{ap}} \boldsymbol{c}_{\boldsymbol{F},\boldsymbol{j}}(\boldsymbol{w},\dot{\boldsymbol{w}}) \prod\limits_{i=1}^{n_1} U_i^{(1),j_i} \prod\limits_{i=1}^{n_2} U_i^{(2),j_{n_1+1}} \\ \tilde{\boldsymbol{C}} = \varkappa \sum\limits_{\boldsymbol{j}\in\mathcal{I}_{ap}} \boldsymbol{c}_{\boldsymbol{C},\boldsymbol{j}}(\boldsymbol{w},\dot{\boldsymbol{w}}) \prod\limits_{i=1}^{n_1} U_i^{(1),j_i} \prod\limits_{i=1}^{n_2} U_i^{(2),j_{n_1+1}} \end{cases} \in \left(\tilde{S}\otimes V\right)^2 \tag{19}$$

with:

- $\mathcal{I}_{ap} = \left\{ \boldsymbol{j} = \left(j_1, \dots, j_{2(n_1+n_2)}\right) \in \mathbb{N}^{2(n_1+n_2)} \quad | \quad \sum_{i=1}^{2(n_1+n_2)} j_i \leq n_f = n_c \right\}$, the index set corresponding to term $\boldsymbol{j}$ of series (19).
- $\boldsymbol{c}_{\boldsymbol{F},\boldsymbol{j}} : \mathbb{R}^n \longrightarrow \mathbb{R}^2$ (respectively $\boldsymbol{c}_{\boldsymbol{C},\boldsymbol{j}} : \mathbb{R}^n \longrightarrow \mathbb{R}^2$), the coefficient associated with term $\boldsymbol{j}$ of series (19).

Next, by adapting the linearization property of the *Chebyshev* polynomials $U_i\, U_j = \sum_{k=0}^{\min(i,j)} U_{|i-j|+2\,k}$ in $]-1,1[$, $\forall (i,j) \in \mathbb{N}^2$, it represents the previous products in the expression (19):

$$\forall \boldsymbol{j} \in \mathcal{I}_s, \quad \prod_{i=0}^{n} U_i^{j_i} = \sum_{\boldsymbol{k} \in \mathcal{I}_s} U_{||\cdots|0-1|+2\,k_0-2|+2\,k_1+\cdots-(i+1)|+2\,k_i+\cdots-(n+1)|+2\,k_n} \quad \text{in} \quad [-1,1] \tag{20}$$

with:

- $\mathcal{I}_s = \left\{ \boldsymbol{k} = \left(k_1, \dots, k_n\right) \in \mathbb{N}^n \quad | \quad k_i \in \left[\left[0, \min\left(||\cdots|1 + \sum_{j=0}^{i} -(j+1)| + 2\,k_j, j+2 \right)\right]\right] \right\}$, the set vector corresponding to term $\boldsymbol{k}$ of the series (20).

Then, by replacing (20) in (19), simplified expressions of forces and moments are obtained:

$$\begin{cases} \tilde{\boldsymbol{F}} = \sum_{\boldsymbol{k} \in \mathcal{I}_k} \boldsymbol{a}_{\boldsymbol{k}}(\boldsymbol{w}, \dot{\boldsymbol{w}})\, \boldsymbol{H}_{\boldsymbol{k}} = \mathcal{H}\, \boldsymbol{a}(\boldsymbol{w}, \dot{\boldsymbol{w}}) \\ \tilde{\boldsymbol{C}} = \sum_{\boldsymbol{k} \in \mathcal{I}_k} \boldsymbol{b}_{\boldsymbol{k}}(\boldsymbol{w}, \dot{\boldsymbol{w}})\, \boldsymbol{H}_{\boldsymbol{k}} = \mathcal{H}\, \boldsymbol{b}(\boldsymbol{w}, \dot{\boldsymbol{w}}) \end{cases} \in \left(\tilde{S} \otimes V\right)^2 \tag{21}$$

with:

- $\boldsymbol{a} : \mathbb{R}^n \longrightarrow \mathbb{R}^m$ (respectively $\boldsymbol{b} : \mathbb{R}^n \longrightarrow \mathbb{R}^m$), the map giving the vector of coefficient associated with term $\boldsymbol{k}$ of previous series (21).

From the expressions (21), it is very easy to identify and retrieve nonlinear stochastic generalized forces without calculating the dot product, thus:

$$\tilde{\boldsymbol{W}}^T = \left\langle \frac{d\boldsymbol{\Phi}^T(L)}{dx}\, \tilde{\boldsymbol{C}} \middle| \mathcal{H} \right\rangle_{S_1', S_2} + \left\langle \boldsymbol{\Phi}^T(L)\, \tilde{\boldsymbol{F}} \middle| \mathcal{H} \right\rangle_{S_1', S_2} = \boldsymbol{a}^T(\boldsymbol{w}, \dot{\boldsymbol{w}})\, \frac{d\boldsymbol{\Phi}(L)}{dx} + \boldsymbol{b}^T(\boldsymbol{w}, \dot{\boldsymbol{w}})\, \boldsymbol{\Phi}(L) \quad \in V^{1\times m} \tag{22}$$

The stochastic generalized forces $\tilde{\boldsymbol{W}}$ are now known without carrying out the numerical integration of the scalar products at each time step. It is now possible to perform a temporal integration of the problem (9) withing reasonable times using the *Runge–Kutta* 4 scheme, with a dispersion rate of $\tau = 5\%$ and numbers n_1 and n_2 of identical *Chebyshev* polynomials for each of the uncertain parameters (k and μ). It is initially necessary to determine the minimum number of polynomials to be chosen (convergence criterion) for each parameter. Fig. 9 presents the temporal evolution of the components of the state vector $\boldsymbol{w}$ for $n_1 = n_2 = 3$. In Fig. 9(a) (and (c) respectively) they are those associated with the first mode of bending in direction y (with respect to z). Likewise, in Fig. 9 (b) (with respect to (d)) those associated with the second mode of bending in direction y (with respect to z). According to these evolutions, it is possible to validate the choice of the number of polynomials selected for each parameter (k and μ), given that the amplitudes of the last two (w_{1j8} et w_{1j9}) for each mode $j \in [\![1,4]\!]$ are very low.

Fig. 10 shows the temporal evolutions of the displacement of the centre of the stator disc s in direction y. In Fig. 10(a), it is the mean $\bar{u}_{s,1}$ (in black), the mean to which is added the standard deviation $\sigma\left[u_{s,1}\right]$ (in blue) and the mean from which is subtracted the standard deviation $\sigma\left[u_{s,1}\right]$ (in red). The expression associated with the mean $\bar{u}_{s,1}$ is written as:

$$\begin{aligned} \bar{u}_{s,1} = \int_\Theta u_{s,1}(\boldsymbol{x}, \cdot)\, d\mathbb{P}_{\boldsymbol{\Xi}}(\boldsymbol{x}) &= \sum_{j=1}^{N} \sum_{\boldsymbol{k} \in \mathcal{I}_k} w_{1jk} \left(\int_\Theta H_{\boldsymbol{k}}(\boldsymbol{x})\, d\mathbb{P}_{\boldsymbol{\Xi}}(\boldsymbol{x}) \right) \phi_{j1}(L) \\ &= w_{110}\, \phi_{11}(L) + w_{120}\, \phi_{21}(L) \quad \in V \end{aligned} \tag{23}$$

For the standard deviation $\sigma\left[u_{s,1}\right]$, the expression is the following:

$$\begin{aligned} \sigma\left[u_{s,1}\right] = \left(\int_\Theta \left(u_{s,1}(\boldsymbol{x}, \cdot) - \bar{u}_{s,1}\right)^2 d\mathbb{P}_{\boldsymbol{\Xi}}(\boldsymbol{x}) \right)^{0.5} &= \left(\int_\Theta \left(\sum_{j=1}^{N} \sum_{\boldsymbol{k} \in \mathcal{I}_k} w_{1jk}\, H_{\boldsymbol{k}}(\boldsymbol{\xi})\, \phi_j^i(L) - \sum_{j=1}^{N} w_{1j0}\, \phi_j^i(L) \right)^2 d\mathbb{P}_{\boldsymbol{\Xi}}(\boldsymbol{x}) \right)^{0.5} \\ = \left(\int_\Theta \left(\sum_{j=1}^{N} \sum_{\boldsymbol{k} \in \mathcal{I}_k \setminus (0,0)} w_{1jk}\, H_{\boldsymbol{k}}(\boldsymbol{\xi})\, \phi_j^i(L) \right)^2 d\mathbb{P}_{\boldsymbol{\Xi}}(\boldsymbol{x}) \right)^{0.5} &= \left(\sum_{j=1}^{N} \sum_{\boldsymbol{k} \in \mathcal{I}_k \setminus (0,0)} w_{1jk}^2\, \phi_{ji}^2(L) \right)^{0.5} \quad \in V \end{aligned} \tag{24}$$

It should be noted that these two final expressions are quite simple. This avoids making numerical integrations which would be much more costly in time. In Fig. 10 (a) temporal evolutions of the mean $\bar{u}_{s,1}$ and the mean plus or minus standard deviation $\bar{u}_{s,1} \pm \sigma[u_{s,1}]$ are presented. In Fig. 10 (b) (respectively (c)), they are limit cycles in the state space that are presented for the following values of

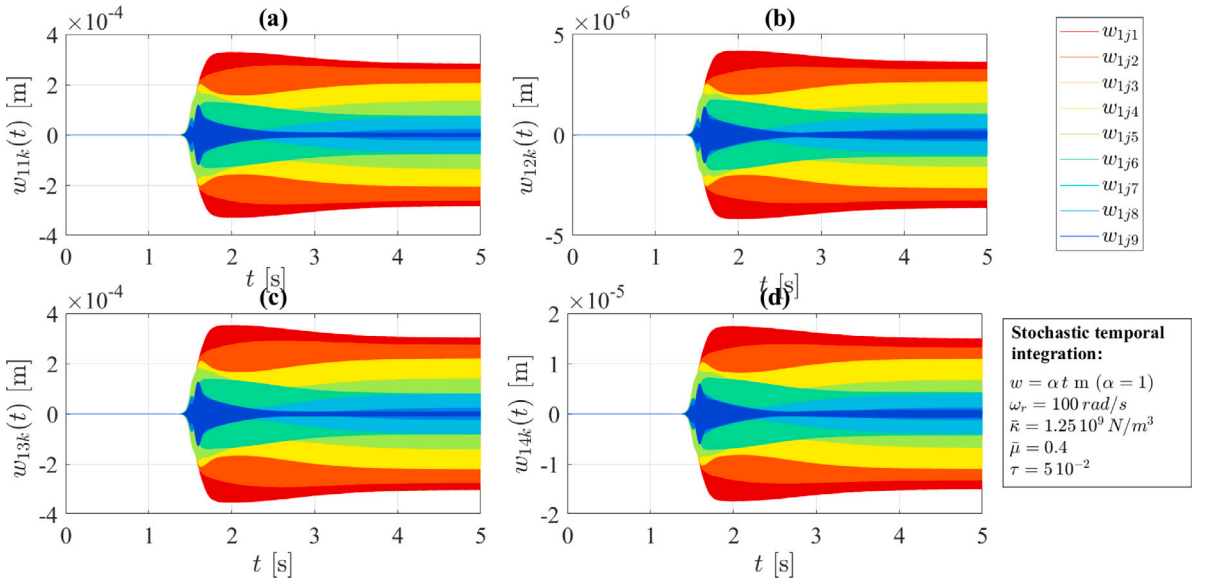

Fig. 9. Temporal evolution of state vector $\boldsymbol{X}$. Components of $\boldsymbol{X}$ denoted w_{ijk}, $k \in [\![1, 9]\!]$ and $j \in \{1; 2; 3; 4\}$, corresponding to the first bending mode of the beam in the direction y (a), the second in direction y (b), the first bending mode of the beam in direction z (c) and the second in direction z (d).

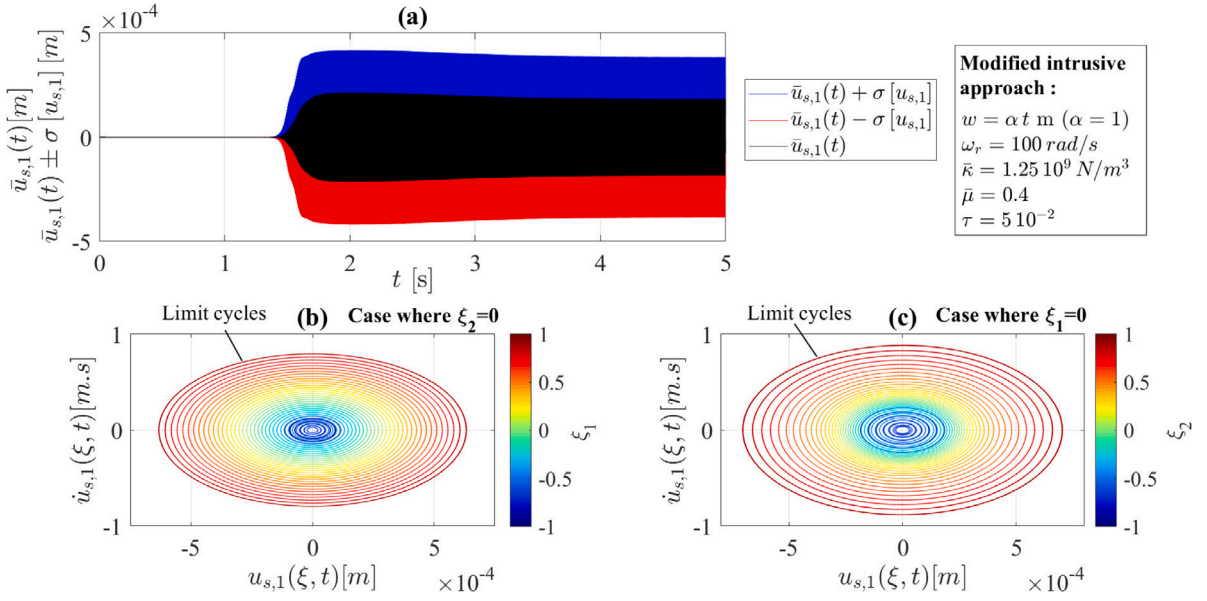

Fig. 10. Temporal evolution of the mean $\bar{u}_{s,1}$, the mean plus or minus the standard deviation $\bar{u}_{s,1} \pm \sigma[u_{s,1}]$ and the limit cycles associated with the displacements $u_{s,1}$. (a) Temporal evolution of $\bar{u}_{s,1}$ (black), the mean plus the standard deviation $\bar{u}_{s,1} + \sigma[u_{s,1}]$ (blue) and the mean plus the standard deviation $\bar{u}_{s,1} - \sigma[u_{s,1}]$ (red). (b) (respectively (c)) temporal evolution of limits cycles in the state space $\mathbb{R}^m$ associated with $u_{s,1}$ and $\dot{u}_{s,1}$ for $\xi_1 \in [-1, 1]$ and $\xi_2 = 0$ (respectively $\xi_2 \in [-1, 1]$ and $\xi_1) = 0$. (For interpretation of the references to colour in this figure legend, the reader is referred to the web version of this article.)

random variables: $\xi_2 = 0$ and $\xi_1 \in [-1, 1]$ (respectively $\xi_1 = 0$ and $\xi_2 \in [-1, 1]$). These data are particularly valuable in the general case of a design of a mechanical system with instabilities induced by friction and presenting uncertainties on certain parameters. The interesting point is that access to these results is obtained in very reasonable times (about 1.5 h) and in a single temporal integration. The difference in computation time is not negligible compared to the classic intrusive approach.

5.3. Comparison with non-intrusive approach using Chebyshev polynomials

In order to validate the modified intrusive approach, the associated results from the modified intrusive approach can be compared to a non-intrusive approach with interpolation (projection L^2). For the latter, it is first necessary to perform temporal integrations

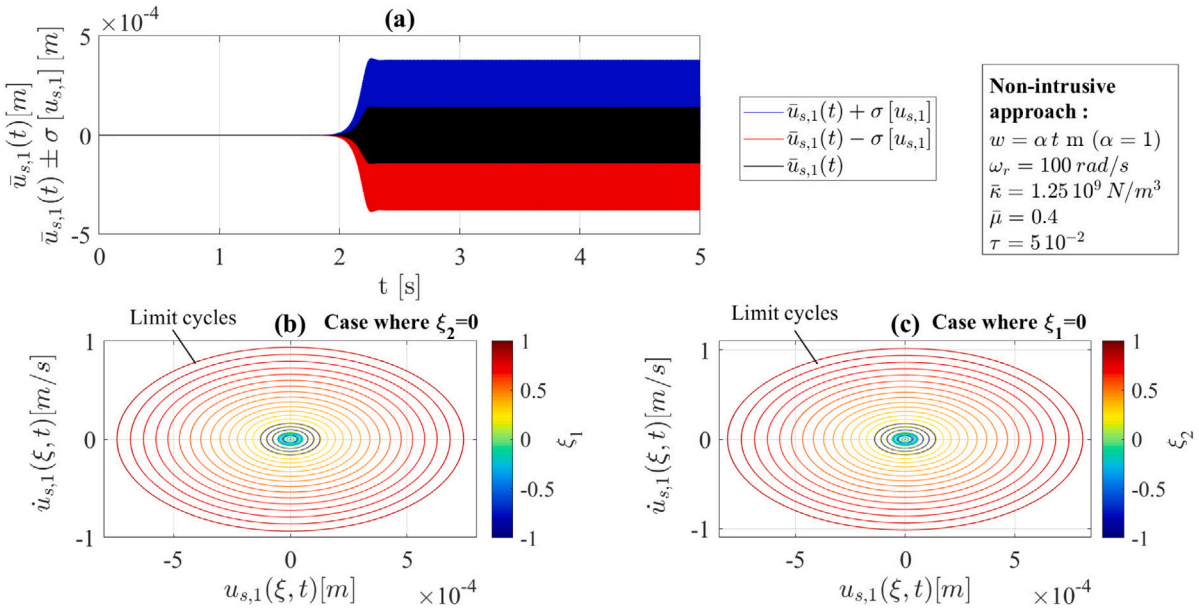

Fig. 11. Temporal evolution of the mean $\bar{u}_{s,1}$, the mean plus or minus the standard deviation $\bar{u}_{s,1} \pm \sigma[u_{s,1}]$ and limit cycles associated with the displacements $u_{s,1}$. (a) Temporal evolution of $\bar{u}_{s,1}$ (black), the mean plus the standard deviation $\bar{u}_{s,1} + \sigma[u_{s,1}]$ (blue) and the mean plus the standard deviation $\bar{u}_{s,1} - \sigma[u_{s,1}]$ (red). (b) ((c) respectively) temporal evolution of limit cycles in the state space $\mathbb{R}^m$ associated with $u_{s,1}$ and $\dot{u}_{s,1}$ for $\xi_1 \in [-1,1]$ and $\xi_2 = 0$ (respectively $\xi_2 \in [-1,1]$ and $\xi_1 = 0$). (For interpretation of the references to colour in this figure legend, the reader is referred to the web version of this article.)

for a set of values of the random variables $\boldsymbol{\xi}$ contained in Θ. An interpolation of the results from these temporal integrations is then performed. For the non-intrusive approach, the weak solution associated with the problem (7) has the following form:

$$\tilde{\boldsymbol{u}} = \boldsymbol{\Phi}\, \boldsymbol{v} \in \tilde{U}_w \tag{25}$$

with:

- $\boldsymbol{v} : (\boldsymbol{\xi}, t) \in \Theta \times T \longmapsto \boldsymbol{v}(\boldsymbol{\xi}, t) \in \mathbb{R}^{2N}$, the first part of the state vector $\boldsymbol{X} \in \mathbb{R}^n$ which is the solution of the problem (9) transformed into a deterministic problem (for this : $n1 = n2 = 1$).

As for the intrusive approach, interesting properties of the Chebyshev polynomial can be used to approximate $\boldsymbol{v}$ at each instant $t \in T$ by interpolation. The use of these polynomials makes it possible to converge uniformly towards the real solution $\boldsymbol{v}$ when the number of polynomials $q \in \mathbb{N}^*$ used tends towards infinity. This allows approximating $\boldsymbol{v}$ as follows:

$$\tilde{\boldsymbol{v}} = \boldsymbol{\mathcal{H}}\, \boldsymbol{w} \in \left(\tilde{S} \otimes V\right)^{2N} \tag{26}$$

with :

- $\boldsymbol{w}^T = \langle \tilde{\boldsymbol{v}} | \boldsymbol{\mathcal{H}} \rangle_{(\tilde{S} \otimes V)^{2N'}, \tilde{S}^{2N \times 2Nq}} = \displaystyle\int_{\Theta} \tilde{\boldsymbol{v}}^T(\boldsymbol{x}, \cdot)\, \boldsymbol{\mathcal{H}}(\boldsymbol{x})\, d\mathbb{P}_{\boldsymbol{\Xi}}(\boldsymbol{x}) \in V^{1 \times 2Nq}$, the projection of $\tilde{\boldsymbol{v}}$ on $\mathcal{H}$.

where : $q = q_1 \times q_2$, corresponding to the number of *Chebyshev* polynomials associated with ξ_1 (q_1) and ξ_2 (q_2). Uniform convergence is guaranteed by choosing particular interpolation points called *Gauss–Chebyshev* points. Using these points, it is possible to approximate $\boldsymbol{w}$ with the following quadrature:

$$\tilde{\boldsymbol{w}}^T = \sum_{i=1}^{Q_1} \sum_{j=1}^{Q_2} \frac{\sin\left(\frac{i\,\pi}{M_1+1}\right) \sin\left(\frac{j\,\pi}{M_2+1}\right)}{\left(M_1+1\right)\left(M_2+1\right)} \tilde{\boldsymbol{v}}^T(\boldsymbol{x}_{ij}, \cdot)\, \boldsymbol{\mathcal{H}}(\boldsymbol{x}_{ij}) \in V^{1 \times 2Nq} \tag{27}$$

with :

- $\left(Q_1, Q_2\right) \in (\mathbb{N}^*)^2$, the number of *Gauss–Chebyshev* points associated with the first (respectively second) random variable ξ_1 (respectively ξ_2) .
- $\forall (i,j) \in [\![1, Q_1]\!] \times [\![1, Q_2]\!], \quad \boldsymbol{x}_{ij} = \left(\cos\left(\frac{i\,\pi}{M_1+1}\right), \cos\left(\frac{j\,\pi}{M_2+1}\right)\right) \in \Theta$, coordinates of *Gauss–Chebyshev* points.

Now, $q = 9$ deterministic temporal integrations associated with $q = 9$ points of *Gauss–Chebyshev*, are realized with the scheme of *Runge–Kutta* 4. Then an interpolation of the results is done using the expression (27). In the Fig. 11, the temporal evolution of the displacement and the limit cycles, corresponding to the centre of the stator disc s in the direction y, are presented and can

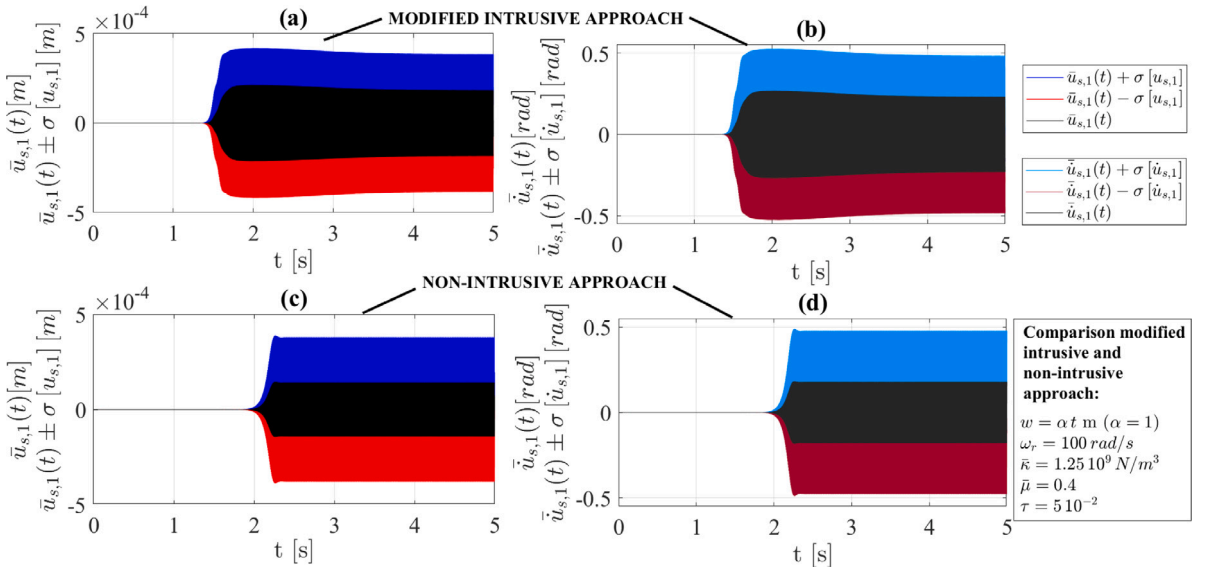

Fig. 12. Comparison of temporal evolutions associated with the mean $\bar{u}_{s,1}$ and $\bar{\dot{u}}_{s,1}$, the mean plus or minus the standard deviation $\bar{u}_{s,1} \pm \sigma[u_{s,1}]$ and $\bar{\dot{u}}_{s,1} \pm \sigma[\dot{u}_{s,1}]$, between the modified intrusive and non-intrusive approaches. (a) ((c) respectively) Temporal evolution of the mean $\bar{u}_{s,1}$, the mean plus the standard deviation $\bar{u}_{s,1} + \sigma[u_{s,1}]$ and the mean plus the standard deviation $\bar{u}_{s,1} - \sigma[u_{s,1}]$. (b) ((d) respectively) Temporal evolution of the mean $\bar{\dot{u}}_{s,1}$, the mean plus the standard deviation $\bar{\dot{u}}_{s,1} + \sigma[\dot{u}_{s,1}]$ and the mean plus the standard deviation $\bar{\dot{u}}_{s,1} - \sigma[u_{s,1}]$.

be compared directly with those in the Fig. 10. Concerning the displacements 11 (a), the extremal amplitudes and the overall shape of the mean $\bar{u}_{s,1}$, mean plus standard deviation $\bar{u}_{s,1} + \sigma[u_{s,1}]$ and mean minus standard deviation $\bar{u}_{s,1} - \sigma[u_{s,1}]$ for modified intrusive 11 (a) and non-intrusive 10 (a) approaches, are very close. There are some differences including a slight time shift that can be observed on the exponential growth of vibrational levels (development of instability). Concerning the limit cycles associated with the values of the random variables (Figs. 11 (b)(c) and Fig. 11 (b) (c)), the amplitudes are also very close. Finally, temporal evolutions between two approaches are presented in the same figure (Fig. 12) to facilitate comparisons. These observations allow to validate the results of the modified intrusive approach. It is also necessary to recall the interest of the modified intrusive approach which makes it possible to obtain results in a single temporal integration, within reasonable delays (4 times faster than the classic intrusive approach) and with more ergonomics than the non-intrusive approach (several deterministic temporal integrations then interpolation of results).

6. Conclusion

This paper described a phenomenological model associated with the physical mechanisms inducing instabilities caused by friction. Uncertainties were taken into account for two of the parameters of this model: the contact stiffness and the coefficient of friction. To properly model the dynamic behaviour of the mechanical system studied, it was necessary to take into account the physical phenomena involved at the interface of the rotor and stator discs and in particular the unilateral contact and adhesion/sliding with friction. The structure of the equations associated with these phenomena is complex, generating resolution times by temporal integration which are already long. In addition, taking into account uncertainties in the model with a classic intrusive approach, induces an additional and not insignificant increase in computation times. Therefore, a modified intrusive approach was presented. This approach comprises two stages and first consists in simplifying the expression of the mechanical actions torsor (forces and moments) at the interface of the rotor and stator discs. To achieve this, an influence study was carried out to identify the variables having a strong influence on the forces and the moments. This study of influence was reinforced by physical considerations and made it possible to develop laws of behaviour between the mechanical action torsors. The polynomial expressions resulting from the simplification can be obtained quickly and the errors made between the approximate expressions and those of the references are very few. Properties of *Chebyshev* polynomials of the second kind were then exploited to calculate the expressions of the generalized stochastic forces, without performing probabilistic numerical integrations of the associated integral terms. Consequently, the temporal integration times could be greatly reduced (4 times faster). The results from the modified intrusive approach were then compared to those of a non-intrusive approach. In the latter, other properties of *Chebyshev* polynomials were also exploited to interpolate the results from deterministic temporal integrations. Small differences were observed between the two approaches for data such as means, standard deviations, and limit cycle amplitudes. Therefore, the results of the optimized non-intrusive approach could be validated. Finally, the modified intrusive approach makes it possible to obtain robust results within very reasonable delays, by performing a single temporal integration and with much more ergonomics than the non-intrusive approach.

Data availability

The authors are unable or have chosen not to specify which data has been used.

References

[1] A.F. D'souza, A.H. Dweib, Self-excited vibrations induced by dry friction, part 2: Stability and limit-cycle analysis, J. Sound Vib. 137 (2) (1990) 177–190.
[2] A.H. Dweib, A.F. D'Souza, Self-excited vibrations induced by dry friction, part 1: experimental study, J. Sound Vib. 137 (2) (1990) 163–175.
[3] N.M. Kinkaid, Olivier M. O'Reilly, Panayiotis Papadopoulos, Automotive disc brake squeal, J. Sound Vib. 267 (1) (2003) 105–166.
[4] James Gordon, Steven Liu, M. Ozbek, A nonlinear model for aircraft brake squeal analysis. II - Stability analysis and parametric studies, in: Dynamics Specialists Conference, in: Structures, Structural Dynamics, and Materials and Co-located Conferences, American Institute of Aeronautics and Astronautics, 1996.
[5] Steven Y. Liu, James T. Gordon, M. Akif Ozbek, Nonlinear model for aircraft brake squeal analysis: Model description and solution methodology, J. Aircr. 35 (4) (1998) 623–630.
[6] Fabrice Chevillot, Jean-Jacques Sinou, Nicolas Hardouin, Louis Jézéquel, Effects of damping on the speed of increase and amplitude of limit cycle for an aircraft braking system subjected to mode-coupling instability, Arch. Appl. Mech. 80 (9) (2010) 1045–1054.
[7] Xavier Lorang, Florence Foy-Margiocchi, Quoc Son Nguyen, Pierre-Etienne Gautier, TGV disc brake squeal, J. Sound Vib. 293 (3–5) (2006) 735–746.
[8] B. Hervé, J. Sinou, H. Mahé, L. Jézéquel, Analysis of friction-induced self-generated vibrations originated from mode-coupling in clutches, Int. J. Pure Appl. Math. 42 (3) (2008) 369.
[9] Benjamin Hervé, J.-J. Sinou, Hervé Mahé, Louis Jézéquel, Analysis of squeal noise and mode coupling instabilities including damping and gyroscopic effects, Eur. J. Mech. A Solids 27 (2) (2008) 141–160.
[10] E. Rabinowicz, The intrinsic variables affecting the stick–slip process, Proc. Phys. Soc. 71 (4) (1958) 668–675.
[11] S.S. Antoniou, A. Cameron, C.R. Gentle, The friction-speed relation from stick–slip data, Wear 36 (2) (1976) 235–254.
[12] Chao Gao, Doris Kuhlmann-Wilsdorf, David D. Makel, The dynamic analysis of stick–slip motion, Wear 173 (1–2) (1994) 1–12.
[13] Chao Gao, Doris Kuhlmann-Wilsdorf, David D. Makel, Fundamentals of stick–slip, Wear 162–164 (1993) 1139–1149.
[14] R.A. Ibrahim, Friction-induced vibration, chatter, squeal, and chaos—Part II: Dynamics and modeling, Appl. Mech. Rev. 47 (7) (1994) 227–253.
[15] R.A. Ibrahim, Friction–induced vibration, chatter, squeal, and chaos—Part I: Mechanics of contact and friction, Appl. Mech. Rev. 47 (7) (1994) 209–226.
[16] R.P. Jarvis, B. Mills, Vibrations Induced by Dry Friction, Proc. Inst. Mech. Eng. 178 (1) (1963) 847–857.
[17] P. Chambrette, L. Jézéquel, Stability of a beam rubbed against a rotating disc, Eur. J. Mech. A Solids 11 (1) (1992) 107–138.
[18] Daniel Hochlenert, Nonlinear stability analysis of a disk brake model, Nonlinear Dyn. 58 (1–2) (2009) 63–73.
[19] Utz von Wagner, Daniel Hochlenert, Peter Hagedorn, Minimal models for disk brake squeal, J. Sound Vib. 302 (3) (2007) 527–539.
[20] Alexy Mercier, Louis Jézéquel, Influence of imperfections on the stability of a multi-disc friction system, J. Sound Vib. (2022) 116712.
[21] Alexy Mercier, Louis Jézéquel, Sébastien Besset, Abdelbasset Hamdi, Jean-Frédéric Diebold, Nonlinear analysis of the friction-induced vibrations of a rotor-stator system, J. Sound Vib. 443 (2019) 483–501.
[22] Alexy Mercier, Louis Jézéquel, Sébastien Besset, Abdelbasset Hamdi, Jean-Frédéric Diebold, Studies on detachment non-linearity at the rotor-stator interface, J. Sound Vib. 468 (2020) 115084.
[23] Fabrice Chevillot, Jean-Jacques Sinou, Nicolas Hardouin, Louis Jézéquel, Simulations and experiments of a nonlinear aircraft braking system with physical dispersion, J. Vib. Acoust. 132 (4) (2010).
[24] A. Renault, F. Massa, B. Lallemand, T. Tison, Experimental investigations for uncertainty quantification in brake squeal analysis, J. Sound Vib. 367 (2016) 37–55.
[25] M. Loève, in: P.R. Halmos (Ed.), Probability Theory I, in: Graduate Texts in Mathematics, vol. 45, Springer New York, New York, NY, 1977.
[26] Christian Soize, A nonparametric model of random uncertainties for reduced matrix models in structural dynamics, Probab. Eng. Mech. 15 (3) (2000) 277–294.
[27] Christian Soize, Maximum entropy approach for modeling random uncertainties in transient elastodynamics, J. Acoust. Soc. Am. 109 (5) (2001) 1979–1996.
[28] Norbert Wiener, The homogeneous chaos, Amer. J. Math. 60 (4) (1938) 897–936.
[29] K.O. Friedrichs, H.N. Shapiro, Integration over Hilbert space and outer extensions, Proc. Natl. Acad. Sci. 43 (4) (1957) 336–338.
[30] Adrian Segall, Thomas Kailath, Orthogonal functionals of independent-increment processes, IEEE Trans. Inform. Theory 22 (3) (1976) 287–298.
[31] Roger G. Ghanem, Pol D. Spanos, Spectral stochastic finite-element formulation for reliability analysis, J. Eng. Mech. 117 (10) (1991) 2351–2372.
[32] Dongbin Xiu, George Em Karniadakis, The Wiener–Askey polynomial chaos for stochastic differential equations, SIAM J. Sci. Comput. 24 (2) (2002) 619–644.
[33] Christian Soize, Roger Ghanem, Physical systems with random uncertainties: chaos representations with arbitrary probability measure, SIAM J. Sci. Comput. 26 (2) (2004) 395–410.
[34] Marc Berveiller, Bruno Sudret, Maurice Lemaire, Stochastic finite element: a non intrusive approach by regression, Eur. J. Comp. Mech./Revue Eur. Méc. Numér. 15 (1–3) (2006) 81–92.
[35] Omar M. Knio, Habib N. Najm, Roger G. Ghanem, A stochastic projection method for fluid flow: I. basic formulation, J. Comput. Phys. 173 (2) (2001) 481–511.
[36] Olivier P. Le Maıtre, Matthew T. Reagan, Habib N. Najm, Roger G. Ghanem, Omar M. Knio, A stochastic projection method for fluid flow: II. Random process, J. Comput. Phys. 181 (1) (2002) 9–44.
[37] Matthew T. Reagana, Habib N. Najm, Roger G. Ghanem, Omar M. Knio, Uncertainty quantification in reacting-flow simulations through non-intrusive spectral projection, Combust. Flame 132 (3) (2003) 545–555.
[38] Andreas Keese, Hermann Matthies, Numerical methods and Smolyak quadrature for nonlinear stochastic partial differential equations, 2003.
[39] Baskar Ganapathysubramanian, Nicholas Zabaras, Sparse grid collocation schemes for stochastic natural convection problems, J. Comput. Phys. 225 (1) (2007) 652–685.
[40] Ma Shao-Juan, Xu Wei, Li Wei, Fang Tong, Analysis of stochastic bifurcation and chaos in stochastic Duffing–van der Pol system via Chebyshev polynomial approximation, Chin. Phys. 15 (6) (2006) 1231.
[41] John C. Mason, Chebyshev polynomials of the second, third and fourth kinds in approximation, indefinite integration, and integral transforms, J. Comput. Appl. Math. 49 (1–3) (1993) 169–178.
[42] Jianping Liu, Xia Li, Limeng Wu, An operational matrix technique for solving variable order fractional differential-integral equation based on the second kind of Chebyshev polynomials, Adv. Math. Phys. 2016 (2016).
[43] Louis Jézéquel, Hugo de Filippis, Alexy Mercier, Analysis and physical interpretation of the uncertainty effect in structural dynamics, J. Eng. Mech. 148 (2) (2022) 04021147.
[44] Hanwei Gao, Louis Jézéquel, Eric Cabrol, Bernard Vitry, Multi-objective robust optimization of chassis system with polynomial chaos expansion method, Eng. Optim. 53 (9) (2021) 1483–1503.
[45] P. Argoul, L. Jézéquel, Improvement of a nonparametric identification procedure used in nonlinear dynamics, J. Appl. Mech. 56 (3) (1989) 697–703.